Airbursts and Cratering Impacts

2024 | Volume 2 | Pages: 1–30 | e-location ID: e20240004
DOI: 10.14293/ACI.2024.0004



Research Article

Modeling airbursts by comets, asteroids, and nuclear detonations: shock metamorphism, meltglass, and microspherules

Allen West[1,*], Marc Young[2], Luis Costa[3], James P. Kennett[4], Christopher R. Moore[5,6], Malcolm A. LeCompte[7], Gunther Kletetschka[8,9] and Robert E. Hermes[10]

[1]Comet Research Group, Prescott, Arizona 86301, USA; [2]College of Humanities, Arts & Social Sciences, Flinders University, Sturt Rd, Bedford Park, South Australia 5042, Australia; [3]Ozen Engineering, Inc., 1210 E Arques Ave #207, Sunnyvale, CA 94085, USA; [4]Department of Earth Science and Marine Science Institute, University of California, Santa Barbara, CA 93106, USA; [5]South Carolina Institute of Archaeology and Anthropology, University of South Carolina, Columbia, SC 29208, USA; [6]SCDNR Heritage Trust Program, Land, Water, and Conservation Division, South Carolina Department of Natural Resources, Columbia, SC 29809, USA; [7]Elizabeth City State University, Center of Excellence in Remote Sensing Education and Research, Elizabeth City, North Carolina 27909, USA; [8]Geophysical Institute, University of Alaska, Fairbanks, Alaska 99775, USA; [9]Faculty of Science, Charles University, Albertov 6, Prague 12843, Czech Republic; [10]Los Alamos National Laboratory (retired), Los Alamos, New Mexico 87545, USA

*Correspondence to: Allen West, E-mail: CometResearchGroup@gmail.com

Received: 27 April 2024; Revised: 27 April 2024; Accepted: 13 May 2024; Published online: 21 June 2024

How to cite: West A., et al. Modeling airbursts by comets, asteroids, and nuclear detonations: shock metamorphism, meltglass, and microspherules. *Airbursts and Cratering Impacts*. 2024 | Volume 2 | Issue 1 | Pages: 1–30 | DOI: 10.14293/ACI.2024.0004

ABSTRACT

Asteroid and comet impacts can produce a wide range of effects, varying from large crater-forming events to high-altitude, non-destructive airbursts. Numerous studies have used computer hydrocode to model airbursts, primarily focusing on high-altitude events with limited surface effects. Few have modeled so-called "touch-down" events when an airburst occurs at an altitude of less than ~1000 m, and no known studies have simultaneously modeled changes in airburst pressures, temperatures, shockwave speeds, visible materials, and bulk material failure for such events. This study used the hydrocode software Autodyn-2D to investigate these interrelated variables. Four airburst scenarios are modeled: the Trinity nuclear airburst in New Mexico (1945), an 80-m asteroid, a 100-m comet, and a 140-m comet. Our investigation reveals that touch-down airbursts can demolish buildings and cause extensive ground-surface damage. The modeling also indicates that contrary to prevailing views, low-altitude touch-down airbursts can produce shock metamorphism when the airburst shockwave or fragments strike Earth's surface at sufficiently high velocities, pressures, and temperatures. These conditions can also produce microspherules, meltglass, and shallow impact craters. Regardless of modeling uncertainties, it is known that bolides can burst just above the Earth's surface, causing significant damage that is detectable in the geologic record. These results have important implications for using shocked quartz and melted materials to identify past touch-down airbursts in the absence of a typical impact crater. Although relatively rare, touch-down events are more common than large crater-forming events and are potentially more dangerous.

KEYWORDS

Airbursts, Comets, Asteroids, Nuclear/atomic detonations, Impact craters, Shock metamorphism, Shocked quartz, Hydrocode modeling, Meltglass, Microspherules

Introduction

Only larger asteroids and comets produce impact craters, whereas most smaller bolides produce airbursts many kilometers above the Earth, usually with little effect. Our investigation focuses on a small subset of bolides that burst at less than ~700 m above Earth's surface. To describe this specific type of near-surface airburst, we adopt the term "touch-down" events (also called Type 2 airbursts [1, 2]) from Van Ginneken et al. [3] Although the characteristics of these objects (e.g., diameter, density, entry angle, and velocity) may be only slightly smaller than those of a typical crater-forming impact, they can still interact with and create extensive damage to Earth's surface [4, 5]. Van Ginneken et al. [3] state that airbursts are the most frequent and most hazardous type of impact event, and yet, such airbursts leave little evidence in the geologic record and, thus, have rarely been studied.

Study objectives

This study is preliminary, and to our knowledge, no one has previously attempted to model touch-down airbursts in this detail with as many parameters. Our primary goal in this study was to use hydrocode to model the potentially damaging effects of touch-down airbursts, mainly by quantifying temperature, pressure, and shock speed. Although no low-altitude touch-down airbursts have been observed in modern times, two high-altitude ones have occurred with damaging ground effects: one over Tunguska, Russia in 1908 and one over Chelyabinsk, Russia in 2013.

Our contribution explores more energetic events that occur at altitudes low enough to produce hypervelocity jets of vapor and impactor fragments that strike Earth's surface. We chose specific modeling parameters to investigate whether touch-down airbursts can (i) occur just above Earth's surface, (ii) eject fragments that strike the ground, (iii) cause significant damage to Earth's surface, (iv) create shallow craters, (v) produce shock metamorphosis in some minerals, (vi) melt surficial sediments to produce meltglass, and (vii) create high-temperature microspherules. We explore bolides of three different sizes (an 80-m asteroid, a 100-m comet, and a 140-m comet) and compare their modeled effects and damage to the Trinity nuclear detonation. In addition, we present 15 other examples of touch-down airbursts using a more comprehensive range of parameters.

It is important to note that the models investigated are based on a very narrow set of parameters. Impactors with the diameters studied here do not have unique solutions and, instead, can have nearly infinite combinations of density, velocity, and angle of entry that will produce significant variations in burst heights and surface damage. We explored only a few of the numerous parameters that can potentially result in near-surface touch-down airbursts.

Even though relatively infrequent, touch-down airbursts are potentially dangerous and more common than typical crater-forming impact events. Boslough [2] concluded that airbursts can produce more surface damage than nuclear explosions of the same yield and, therefore, are more dangerous than previously assumed. The increased damage is partially due to the difference between a moving bolide with significant downward momentum and a stationary nuclear detonation, such as the Trinity atomic detonation. We explore this issue with our hydrocode models.

This preliminary investigation uses a limited suite of parameters, and we acknowledge considerable uncertainty about the effects of touch-down airbursts, especially since none have been scientifically documented in modern times. However, it is crucial to understand these types of touch-down airbursts and the evidence they may leave in the geological record. The primary purpose of this investigation is to test whether these observations are consistent with modeling experiments.

Airbursts: bolide fragmentation

Most studies conclude that during airbursts at all altitudes, the incoming comet or asteroid is mostly vaporized [6, 7]. However, some fragments from many airbursts commonly reach the ground surface, as in the following examples, most of which occurred at high altitudes and were not touch-down airbursts. On the other hand, for touch-down or Type 2 airbursts, the kinetic energy of the airburst may be high enough to eject fragments at hypervelocities, producing shallow craters. In this study, we explore bolide fragmentation and crater formation.

In the first high-altitude example, the airburst of the Tagish Lake meteorite (4 to 6 m in diameter, weighing 56 tonnes) occurred ~29 km high above British Columbia, Canada, in January 2000. It produced an elliptical strewn field 5 × 16 km long containing >10,000 fragments up to ~2.3 kg, each reaching the surface at terminal velocities [8, 9].

In another example, fragments of the Sikhote-Alin iron meteorite struck Siberia in 1947, distributing ~8500 pieces totaling more than 23,000 kg across 1.6 square km. This event produced more than 100 impact craters ranging from 0.5–26 m in diameter [10].

Also, Argentina's Campo del Cielo meteorite field contains >100 meteorites that formed craters up to 26.5 m in diameter and 6 m in depth. For the Sikhote-Alin and Campo del Cielo airbursts, shock pressures were sufficiently energetic to produce shock-generated craters in unconsolidated surficial sediments.

Thus, fragmentation during airbursts appears to be common, regardless of whether the bolide is a comet or an asteroid and whether it occurs at a high or low altitude. The above evidence shows that bolide fragments from airbursts can reach the Earth's surface, sometimes causing surface damage and shallow craters. This observation is one of the critical issues that we test with this modeling investigation.

Airbursts: meltglass and microspherules

Meltglass and microspherules occur in many common terrestrial and anthropogenic formations and thus, it is not

always easy to differentiate them from impact examples, especially in the case of touchdown impacts without significant cratering. To distinguish the difference, shocked quartz and diaplectic glasses are decisive criteria. The production of meltglass and microspherules in airbursts, a central issue explored here, is described in the examples below.

Boslough and Crawford [5] described the theoretical process by which airbursts can produce meltglass. This process is important, so we quote their comment in its entirety. For some airbursts "*with a kinetic energy above some threshold, the hot jet of vaporized projectile (the descending 'fireball') makes contact with the Earth's surface, where it expands radially. During the time of radial expansion, the fireball can maintain temperatures well above the melting temperature of silicate minerals, and its radial velocity can exceed the sound speed in air. We suggest that the surface materials can ablate by radiative/convective melting under these conditions, and then quench rapidly to form glass after the fireball cools and recedes.*"

The first meltglass-producing example is proposed at Tall el-Hammam in the Jordan Valley northeast of the Dead Sea, where a 50-m to 75-m touch-down airburst is proposed to have destroyed an ancient city ~3600 years ago [11]. The high-temperature event produced meltglass, melted pottery, and melted mudbricks, some of which contain the imprints of plant material.

In another proposed airburst example, Osinski et al. and others [12–14] reported large quantities of meltglass produced ~145,000 years ago along the shores of the Dakhleh Oasis in Egypt. The glass was discovered near the oasis at six locations separated by >40 km across ~400 km^2. This glass contains melted silica (lechatelierite, which forms at >1700 °C) that co-occurs with shock-fractured quartz and microspherules [12, 15]. Notably, Dakhleh glass contains the preserved imprints and fossil remains of plants onto which the molten glass fell. These impressions are similar to those observed on the melted roofing clay from Tall el-Hammam [11].

Similarly, a large meltglass strewn field from a proposed low-altitude airburst has been reported in a 75-km-long narrow corridor of Chile's Atacama Desert [16–18]. The studies report twisted and folded silicate glasses up to 4 m in diameter and up to 15–25 cm thick [19], containing meteoritic grains [18] and shocked quartz grains [19]. Boslough et al. [20] attribute the 75-km-long field of meltglass to multiple low-altitude airbursts from fragments of a single comet. As with other airburst sites, this glass contains fossil imprints of plants on the surface at the time of the airburst.

Meltglass and microspherules produced by multiple hemispheric airbursts has been proposed for several sites at the 12,800-year-old Younger Dryas boundary (YDB) in Syria [21–23], Venezuela [24, 25], Pennsylvania [26], South Carolina [26], New Jersey [27], and New York [28]. The site in Syria at Abu Hureyra also displays plant imprints in meltglass, similar to imprints found at other YDB airburst sites.

In another potential airburst example, the Libyan Desert glass field is attributed to a cosmic event ~29 million years ago. The field extends across ~6500 km^2 of the desert in Egypt [29] and is estimated to contain 1400 tonnes of meltglass [30], microspherules [31, 32], and shocked quartz [33, 34].

To explore a possible airburst origin of Libyan Desert glass, Svetsov et al. [30] developed a hydrocode model demonstrating that the glass could have formed during an airburst rather than a typical crater-forming impact. Likewise, Boslough and Crawford [5] developed a hydrocode airburst model for Libyan Desert glass using a 120-m-diameter sphere to represent an asteroid with kinetic energy of about 108 megatons and a maximum temperature of 5800 K. The caption of Boslough and Crawford's Fig. 8 [5] states that the model produced a low-altitude airburst during which the high-temperature jet descended to Earth's surface, and their figure also shows that the airburst excavated a multi-m-deep crater [5]. Importantly, Boslough and Crawford state: "*…the resulting fireball (which contains air and ablated meteoritic material at temperatures exceeding the melting temperature of quartz) makes direct contact with the surface over a 10 km diameter area for more than 10 s after the explosion.*" [5]. Thus, their model shows that low-altitude airbursts can produce craters and meltglass. We further investigate this meltglass-forming process using our hydrocode models.

Hydrocode modeling

Hydrocode programs are commonly used for impact simulations [1, 6, 35–41]. For this study, we first modeled airbursts using the Earth Impact Effects Program (EIEP) by Marcus et al. [42] and Collins et al. [39, 40] It is important to note that those authors caution that the methodology implemented in the EIEP is simplistic. Furthermore, Marcus et al. [42] emphasized that the results have significant uncertainties due to the limited understanding of impacts and airbursts. Even so, the EIEP and other modeling work by Collins et al. [39, 40, 43] is cited and used in hydrocode simulations for impact modeling [37, 44–47] and has been reported to produce consistent results [47].

After entering the results from EIEP, we made all other key calculations using Autodyn-2D (Ansys, Inc.), a hydrocode computer program previously used for modeling hypervelocity impact investigations [48–59]. We modeled airbursts by one asteroid (80 m in diameter) and two comets (100 and 140 m), each with different densities (~1500, ~1000, and ~500 kg/m^3, respectively) and different velocities prior to the airburst (17, 30, and 51 km/s, respectively). In addition, we produced a model of the Trinity nuclear detonation. The Trinity modeling was conducted only using Autodyn because the EIEP cannot model a static nuclear explosion. The input values (e.g., equations-of-state and

material parameters) are provided below in Methods and in Supporting Information.

Autodyn is especially useful for modeling complex physical phenomena, including simultaneous interactions of liquids, solids, and gases, and for calculating phase transitions in multiple modeled materials. It is useful for modeling pressure, temperature, shock speed (defined here as the airburst-induced pressure wave that propagates through various materials, often at hypersonic velocities), and bulk material failure (defined as the point at which strain on a material exceeds a specified pressure value in the tensile direction).

In this study, temperatures are not fully quantitative because of the inherent difficulties in accurately determining extreme temperatures under chaotic conditions. The Autodyn program can account for some types of energy (e.g., kinetic, strain, and contact) but is unable to accurately calculate how some parameters affect temperature (e.g., plasma chemistry/physics and thermal radiation), potentially leading to modeled temperatures that are too high. Thus, for this study, Autodyn's calculated temperatures are semiquantitative and primarily shown to illustrate the evolution of convection currents.

Concerning Autodyn's utility, Pierazzo et al. [60] compared Autodyn with other commonly used modeling codes, including SOVA, SPH, iSALE, CTH, and ALE3D, and then compared those models with physical experiments. Those authors found Autodyn to agree well with the other code models and the experimental results [60]. They found that increasing the impact velocity adversely affected the accuracy of predicted peak pressures, but even so, they found Autodyn and other codes to be in good overall agreement with each other and with real-world experiments [60]. Baldwin et al. [49] concluded that Autodyn was able to replicate their laboratory impact experiments, and they used it to model large planetary impacts. However, both studies focused only on typical crater-forming impacts rather than airbursts.

Results and interpretations

Using the EIEP and Autodyn, we modeled the effects of four airbursts with a range of bolide diameters from 80–140 m, selectively chosen because the models produce touch-down airbursts, during which the hypervelocity jet intersects Earth's surface. However, the effects of airbursts can vary widely depending upon a bolide's diameter, density, velocity, angle of entry, and burst height [6, 7, 36, 61, 62].

We calculated multiple metrics (pressure, semiquantitative temperature, shock speed, visible representation, and material bulk failure) within a specific interval (ms) to illustrate a wide range of potential effects. The output includes images and videos (some shown below), which were generated to display the evolution of airbursts over time, including pressure, semiquantitative temperature as convection currents, shock speed, and visible conditions. Also illustrated is bulk failure, a metric indicating that some material has undergone damage exceeding the point at which material strain exceeds a specified pressure value in the tensile direction. This failure signifies that the formerly dense material has become hydrodynamic (i.e., pulverized, fractured, or amorphized).

Testing modeling accuracy

It is challenging to determine modeling accuracy related to touch-down airbursts because of a lack of scientifically recorded direct observations for comparison. However, there are two modern observed high-altitude airbursts to compare using the EIEP.

Tunguska, Russia (Table 1)

The blast yield of this 1908 airburst is estimated at ~10–15 megatons of TNT equivalent with a burst altitude of ~5–10 km [63–66]. The airburst generated a shockwave that toppled or snapped >80 million trees across ~2000 km^2 in a radial pattern from ground zero [63–66]. Estimated surface wind velocities were ~40–70 m/s (144–250 km/h), greater than an EF-3 tornado [37], and the airburst ignited fires that

Table 1: Tunguska, comparison of actual to modeled values.

Tunguska	EIEP values	Actual values	Factor	Source
Diameter	60 m			Marcus et al. 2004
Density	2700 kg/m^3			Marcus et al. 2004
Velocity	20 km/s	20-40 km/s		Marcus et al. 2004
Entry angle	45°	5°-45°		Marcus et al. 2004
Airburst height	5.74 km	6-12 km	>1.1×	Jenniskens et al. 2019
Airburst energy	13.4 Mt	10-15 Mt	=	Jenniskens et al. 2019
Fragments struck Earth	Yes	Yes?	≈	Zlobin 2018
Overpressure	130-260 kPa	10-30 kPa	~0.23×	Jenniskens et al. 2019
Max wind velocity	211 m/s	40-70 m/s	~0.33×	Jenniskens et al. 2019
Trees, 90% blown down	Yes	Yes	=	Jenniskens et al. 2019

First, we entered the top four variables into the EIEP using the same values presented online by the creators of the EIEP, Marcus et al. [145], in their use of the EIEP for Tunguska. Next, we compared the EIEP output with known or estimated values for the Tunguska high-altitude airburst. Actual values were either equal ("="; three values) or different by ~0.23–1.1 times (three values), a reasonably similar comparison.

consumed ~500 km^2 of forest [64]. The blast from this relatively small high-altitude airburst is reported to have killed ~3 of the ~30 people near ground zero, and nearly everyone experienced severe burns within an eight-km radius. [67] The comparison between the actual values and those modeled in the EIEP shows good correspondence (Table 1).

Chelyabinsk, Russia (Table 2)

In 2013, a ~29.7-km-high, ~500-kt airburst [6, 36, 68–70] occurred over Chelyabinsk, Russia. The blast ejected numerous meteorite fragments, two of which weighed 64.7 and 540 kg [71]. They struck Earth's surface at low terminal velocities, with the largest creating a 9-m diameter hole in a frozen lake. Even though this airburst occurred high above the Earth's surface, the shockwave injured nearly 1500 people on the ground, mostly from flying glass and other debris. The comparison between the modeled and actual values (Table 2) shows good correspondence. Given the lack of detailed information about touch-down airbursts, using EIEP in this study is acceptable as a first-order approximation.

Trinity: height, 31.4 m; 24.8 kt; plutonium, 19.8 g/cm^3; tower, 9.7 g/cm^3; ground, 2.64 g/cm^3 (Figures 1–7).

Asteroid: 80 m wide; 13.7 Mt, velocity 17 km/s; density 1500 kg/m^3; entry 90°; initial fragmentation at 72.5 km; burst height 662 m (Figures 8–14).

Comet: 100 m wide; 57.9 Mt, velocity 30 km/s; density 1032 kg/m^3; entry 90°; initial fragmentation at 89.2 km; burst height 203 m (Figures 15–21).

Comet: 140 m wide; 236 Mt, velocity 51 km/s; density 530 kg/m^3; entry 90°; initial fragmentation at 108.0 km; burst height 193 m (Figures 22–28).

Summary of modeling results

Table 3 below lists the modeling results included in the figures above.

Other modeling parameters and results

The above results illustrate touch-down airbursts by three bolides: an 80-m asteroid, a 100-m comet, and a 140-m comet. To estimate how rare such events might be, we used the EIEP to explore the effects of using different bolide entry angles (90°, 60°, 45°, 30°, and 15°) while keeping density and entry velocity the same (Table 4). In addition, we selected bolide diameters that would produce nearly the same burst heights for each example. Doing so caused the bolides to vary up to ~4× larger in diameter and up to ~60× in energy (Mt). In another test, we retained the original diameters, densities, and entry velocities but changed the entry angle to 45°. This change in angle resulted in high-altitude airbursts rather than touch-down events.

Notably, the results of these experiments suggest that innumerable variations in entry angles and bolide diameters can produce essentially the same low-altitude burst heights of <700 m. These experiments also demonstrate that innumerable possible variations of all parameters can produce higher burst heights without producing touch-down airbursts. Thus, although touch-down airbursts are a small subset of all airbursts at all altitudes, the evidence discussed here suggests they are not statistically rare.

Discussion

Modeled results for Trinity

Trinity nuclear detonation

The Trinity nuclear detonation provides valuable observational data for further testing of the modeling accuracy.

Table 2: Chelyabinsk, comparison of actual to modeled values.

Chelyabinsk	EIEP values	Actual values	Factor	Source
Diameter	22 m	--	--	Marcus et al. 2004
Density	3300 kg/m^3	--	--	Marcus et al. 2004
Velocity	19 km/s	--	--	Marcus et al. 2004
Entry angle	20°	--	--	Marcus et al. 2004
Airburst height	28.4 km	27-33 km	=	Brown et al. 2013
Airburst energy	350 kt	400-600 kT	>1.1×	Brown et al. 2013
Fragments struck Earth	Yes	Yes	=	Brown et al. 2013
Overpressure	2160 Pa	2600-4200 Pa	>1.2×	Brown et al. 2013
Max wind velocity	2.54 m/s	5.5-9.5 m/s	>2×	Brown et al. 2013
Shattered windows	Yes	Yes	=	Brown et al. 2013

First, we entered the top four variables into the EIEP using the same values presented online by Marcus et al. [145] in their use of the EIEP for Chelyabinsk. Next, we compared the EIEP output with known or estimated values for the Chelyabinsk high-altitude airburst. For six key parameters, actual values were either equal (three values) or different by ~1.1–2.0 times (three values), a reasonably similar comparison.

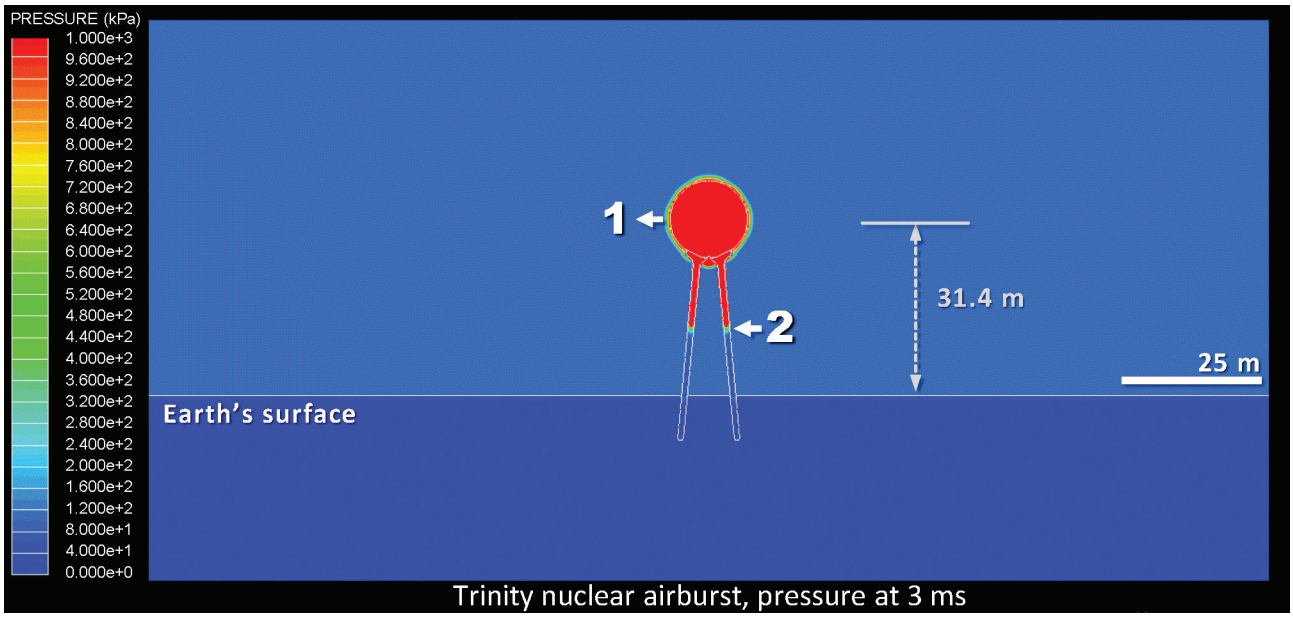


Figure 1: Trinity, pressure at 3 ms. The resolution of 0.28 × 0.28 m is sufficient to model the Trinity bomb and tower legs. However, we modeled them several times larger for greater visibility but still used actual density and energy inputs. Thus, the model results are comparable to the observed results. **#1)** The Trinity bomb was mounted ~31.4 m high on a metal tower 30.48 m tall (100 ft.). The nuclear fireball is ~16 m wide at 3 ms. **#2)** Legs of the tower (not to scale) extend ~6 m into the Earth beneath the tower. This model shows that blast pressures (red) are transmitted down the tower legs. The modeled pressure = ~60 GPa in the fireball and ~5 GPa at the top of the metal tower legs; shock speed = 25,000 m/s inside the fireball. Semiquantitative temperature = ~4000 K. The field of view is 200 × 100 m. ***Click the bar below for the Pressure video.***

Click for Video: Trinity, Pressure

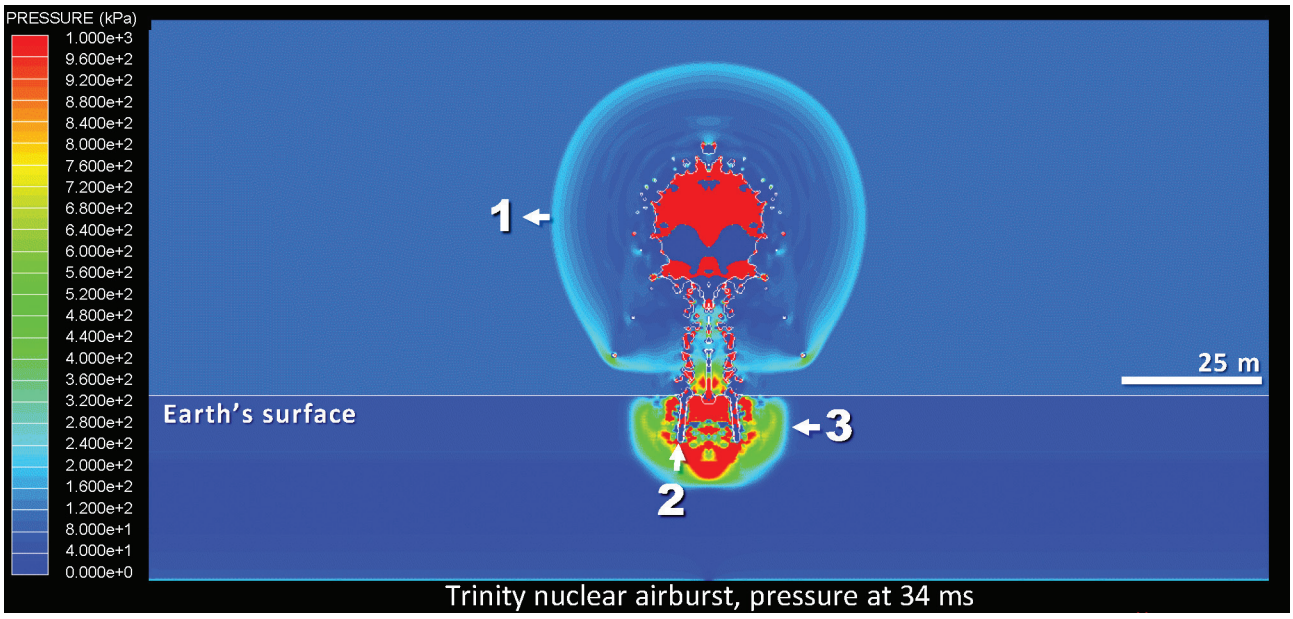


Figure 2: Trinity, pressure at 34 ms. **#1)** The touch-down nuclear fireball is ~55 m wide at 34 ms. **#2)** High pressures >1 GPa are transmitted through the tower legs, and **#3)** into the Earth below the tower. The modeled pressures are sufficient to produce shock metamorphism. Maximum modeled pressure = 17 GPa; shock speed = 4600 m/s; temperature = ≥300,000 K. The field of view is 200 × 100 m.

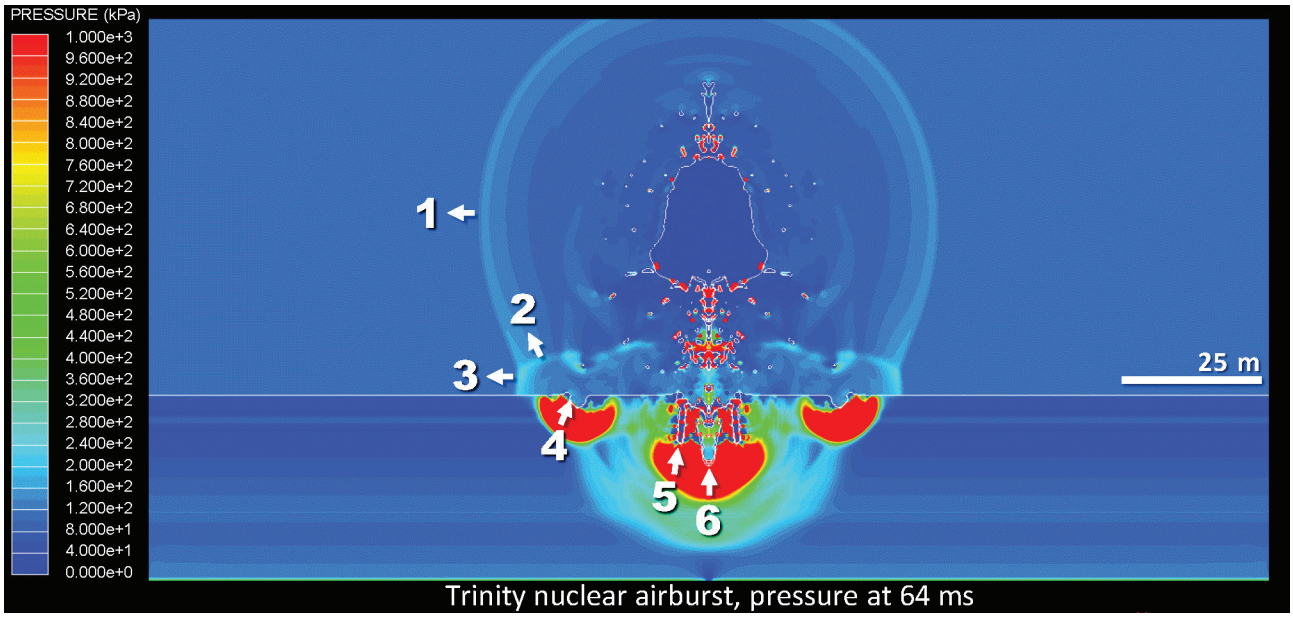


Figure 3: Trinity, pressure at 64 ms. **#1)** The nuclear fireball is ~82 m wide. Maximum shock speed = 4600 m/s. Upon contacting the ground, the blast wave produces **#2)** a reflection wave that rebounds upward and **#3)** a base surge that expands laterally. **#4)** High-velocity fragments from the bomb produce multiple craters up to 2 m deep, spread across ~55 m of the ground surface. **#5)** The pressure damages the buried tower foundations. **#6)** Fragments of the bomb and tower create a ~12-m deep crater under the tower. Maximum pressure on the surface is ~15 GPa, sufficient to produce shocked quartz [73]. Maximum temperatures are higher than the vaporization temperature of quartz.

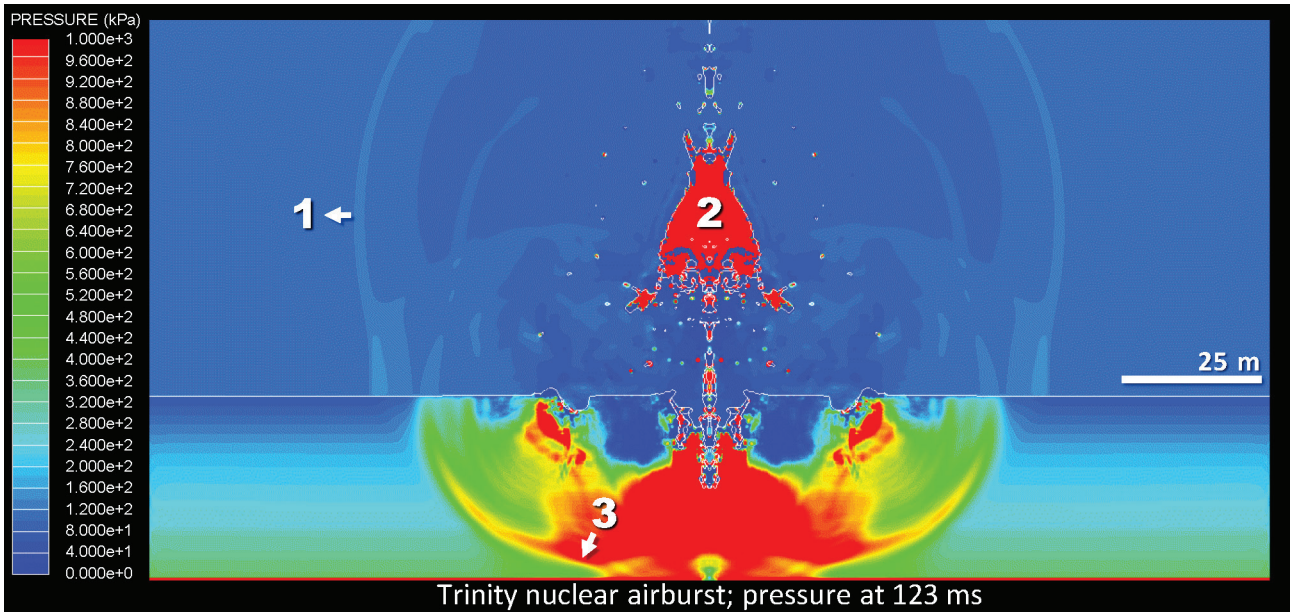


Figure 4: Trinity, pressure at 123 ms. **#1)** The fireball is ~127 m in diameter. **#2)** Maximum pressure = 8 GPa within the fireball. **#3)** A pressure wave (0.2 GPa) propagates into the earth. The maximum shock speed is ~4300 m/s, and the maximum model temperature was ~300,000 K, matching the previously reported maximum temperature [81].

Pressure Table 5 compares observational data for the Trinity nuclear test with those from the Autodyn model. Measurements from ground sensors distributed across the Trinity site were reported by Marley et al. [72], who observed a maximum pressure of 76,000 kPa (0.076 GPa) on the ground surface 63 m from the fireball's center. This measurement is similar to Autodyn's modeled ground pressure of 100,000 kPa (0.10 GPa) at ~63 m. These values differ by only 0.76 times (Table 5).

However, the ground measurements do not account for the higher pressures on the ground surface generated by fragments of the bomb and the tower. For those conditions,

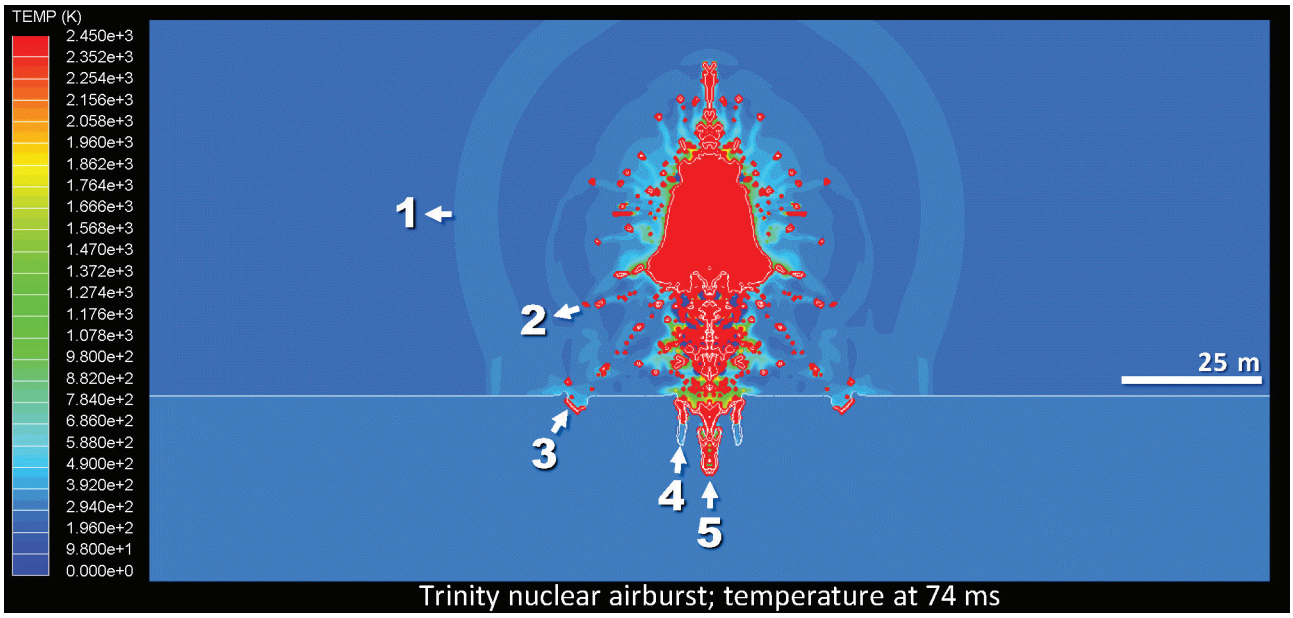


Figure 5: Trinity, semiquantitative temperature (shows convection currents) at 74 ms. **#1)** The touch-down nuclear fireball is ~92 m wide. Maximum shock speed = ~4500 m/s. **#2)** Molten fragments of the bomb and sediment (red) are ejected or drawn into the rising fireball plume. Only a few fragments are modeled for Trinity and the other airbursts described below; in reality, there would be thousands to millions of fragments. **#3)** Craters formed by the impact of fragments are up to 10 m deep and span ~55 m. **#4)** Temperatures near the tower legs and **#5)** beneath the tower exceed the boiling point of quartz. Maximum pressure = ~10 GPa, sufficient to shock quartz grains. ***Click the bar below for the Temperature Video.***

Click for Video: Trinity, Temperature

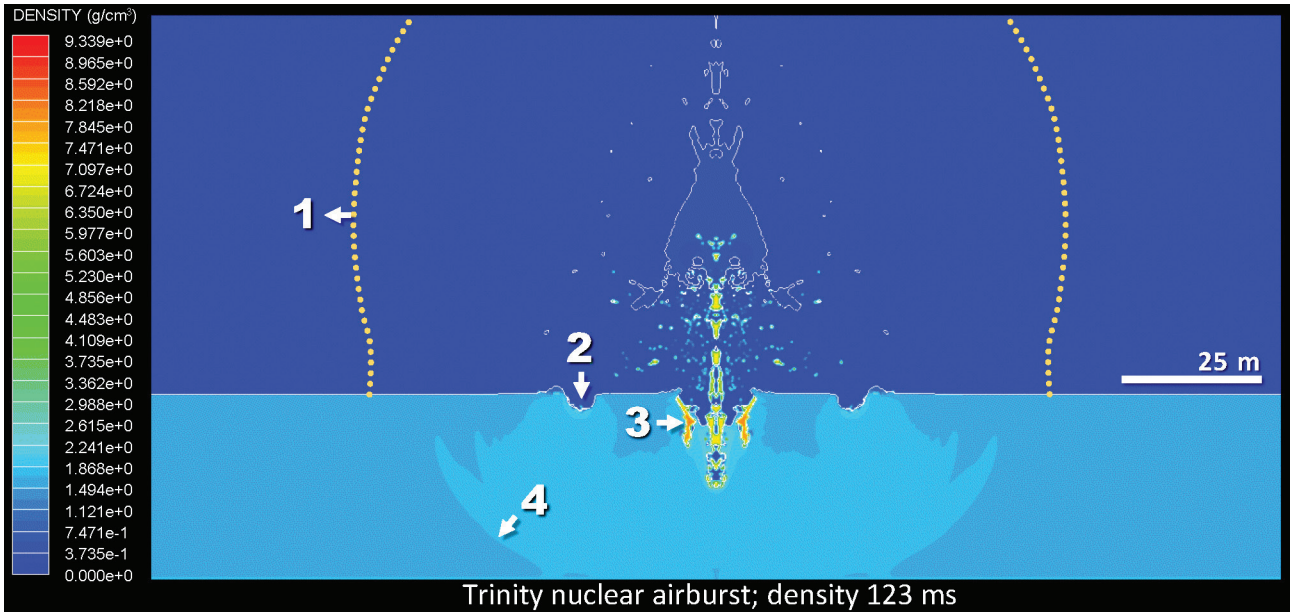


Figure 6: Trinity, density at 123 ms. **#1)** The fireball is 127 m wide. **#2)** Bomb and tower fragments produce ~3-m-deep craters on the ground surface at the arrow. **#3)** The fragments create a >5-m-deep crater beneath the bomb. Below the tower, the high pressure compresses the sandy, unconsolidated sediment ~3.5× from ~2.64 g/cm^3 to ~9.34 g/cm^3. **#4)** This densifying shockwave continues downward through the substrate, further compressing the sediment.

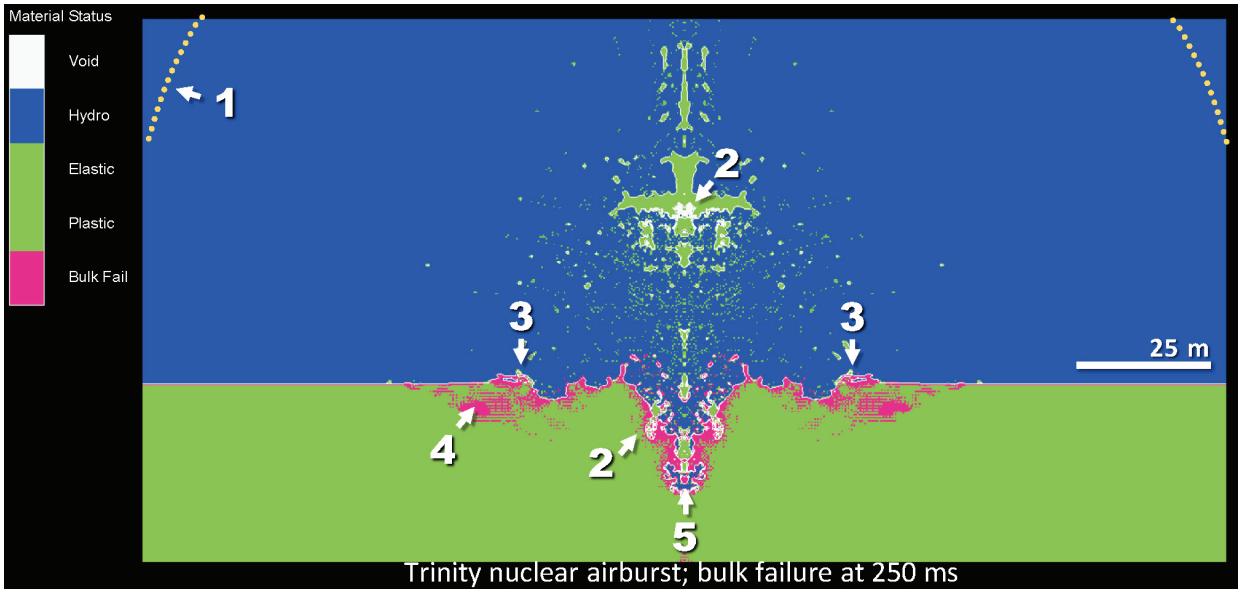


Figure 7: Trinity, bulk failure at 250 ms. **#1)** The fireball is 235 m wide (wider than the field of view). **#2)** The white areas at the fireball's center and near the deepest part of the crater, listed as "void," represent near-vacuum conditions. **#3)** The cratered area is ~75 m wide with an upturned rim. **#4)** High pressures and temperatures cause the bulk sediment to become broadly plastic/elastic (green). Note that "elastic" means reversibly flexible with the potential to reheal; "plastic" means irreversibly flexible and cannot reheal. In and around the craters, sediment experiences bulk failure and is pulverized or amorphized (red). **#5)** Melted bomb parts and sediment line the walls of craters that are up to 20 m deep under the tower and ~3 m deep further away. Melted/plastic bomb parts and sediment (red and green) are ejected from the crater. The maximum modeled pressure = ~5 GPa, and the maximum shock speed = ~4200 m/s. ***Click the bar below for the Bulk Failure video.***

Click for Video: Trinity, Bulk Failure

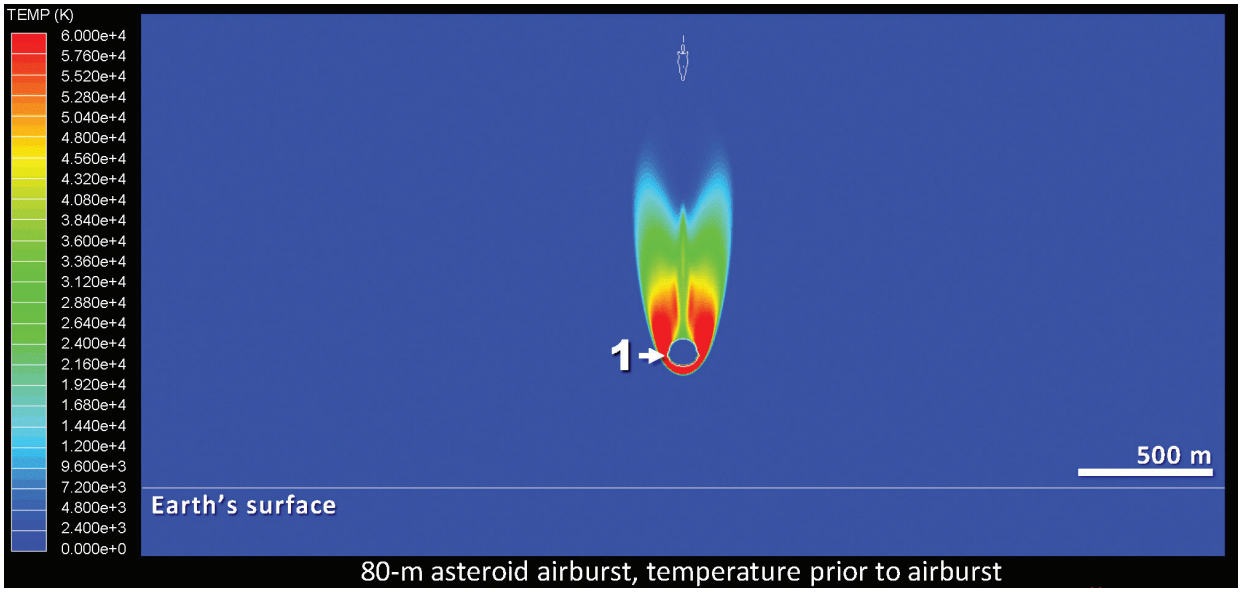


Figure 8: 80-m asteroid, semiquantitative temperature (shows convection currents) before airburst. The asteroid is modeled as a deformed solid sphere but, in actuality, is a swarm of co-moving fragments and vapor. Atmospheric friction causes the swarm to assume a fragmented, pancake-like shape, although the total airburst energy remains unchanged. **#1)** The approximate modeled temperature in front of and in the wake of the asteroid before the airburst is ~60,000 K. This value is consistent with studies by Silber et al. and others [99, 100, 146], who reported meteoroid temperatures ranging up to 95,000 K. Zhilyaev et al. [100] also modeled temperatures of up to 100,000 K. However, the temperature in the flow field behind the bolide may exceed that value. Field-of-view is 4000 × 2000 m. Estimated asteroid recurrence interval = ~1700 years [40, 42], although this interval applies to all 80-m impact events, not just airbursts. ***Click the bar below for the Temperature video.***

Click for Video: 80-m, Temperature

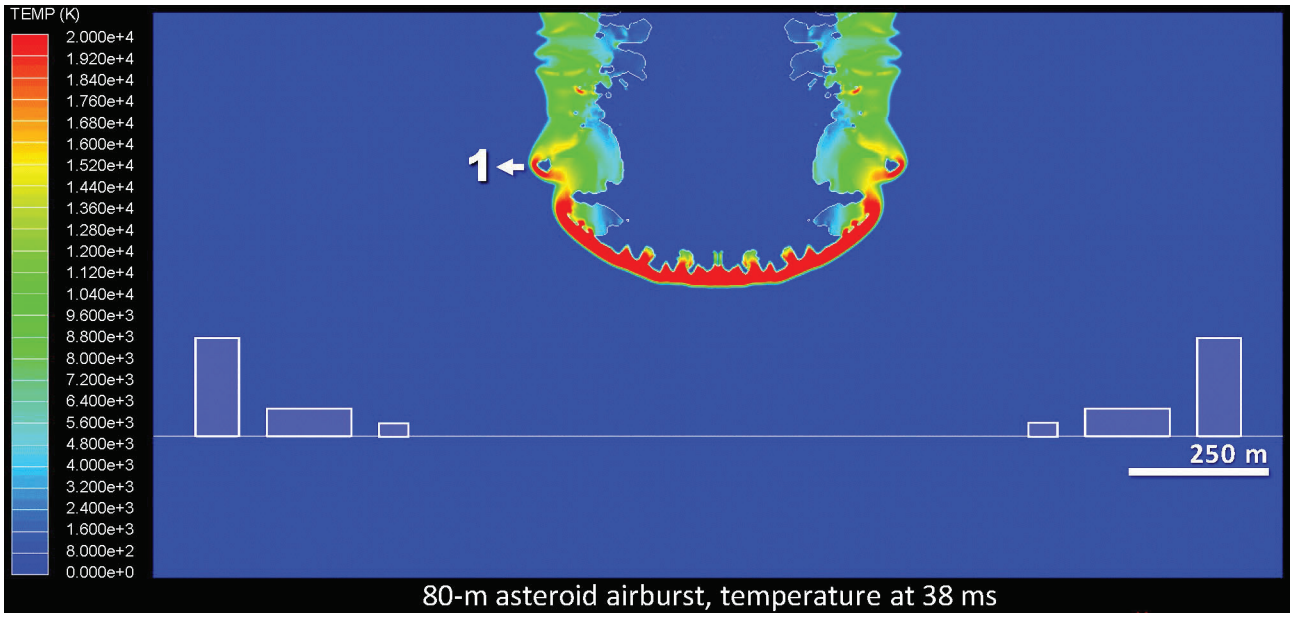


Figure 9: 80-m asteroid, semiquantitative temperature (shows convection currents) at 38 ms. **#1)** The asteroid airburst is ~680 m wide. Maximum pressure = ~2 GPa, maximum shock speed = 13,000 m/s, and maximum approximate temperature = 32,000 K. The model of a high-rise building is 75 × 175 m; the model of the middle building is 50 × 150 m; and the smallest building is 25 × 50 m.

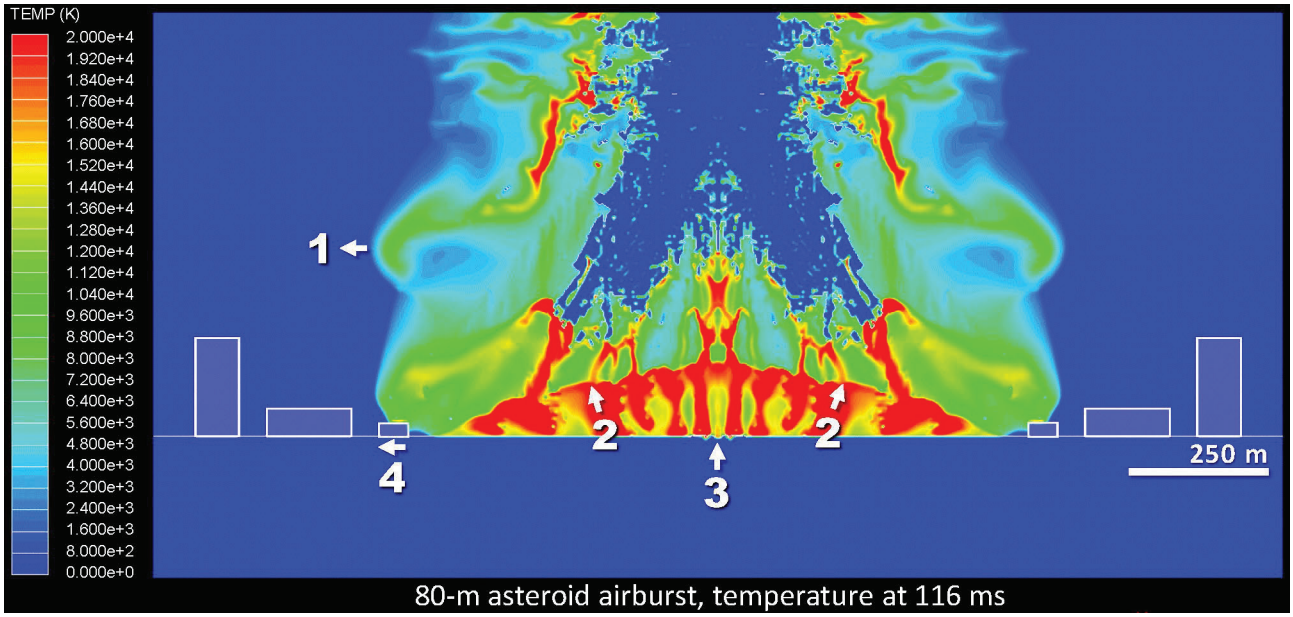


Figure 10: 80-m asteroid, semiquantitative temperature (shows convection currents) at 116 ms. **#1)** The asteroid airburst is ~1,220 m wide. Maximum ground surface pressure = 15 GPa, sufficient to produce shocked quartz. The maximum shock speed = 7400 m/s. **#2)** The expanding airburst produces a reflection wave after striking the Earth. **#3)** The high-velocity, high-pressure wave melts surface sediment, and fragments create shallow craters. **#4)** High-temperature shockwaves at >8000 K engulf the smallest of six modeled buildings.

Hermes et al. [73] reviewed and summarized reports that key minerals display the shock effects of the extreme pressures generated in the Trinity nuclear test: 25 to 60 GPa for vesiculated feldspar [74], 8 to 10 GPa for shocked quartz [75, 76], 7 to 10 GPa for shocked zircon [77], 8 GPa based on the fractionation of zinc [78], and 5 to 8 GPa based on quasi-crystalline minerals in trinitite [79]. Autodyn's modeled pressure range of 5 to 60 GPa matches these minerals' reported range of 5 to 60 GPa. These high pressures likely reflect those generated by the nuclear shockwave by impacts by bomb and tower fragments with the ground surface and are sufficiently high to produce the observed

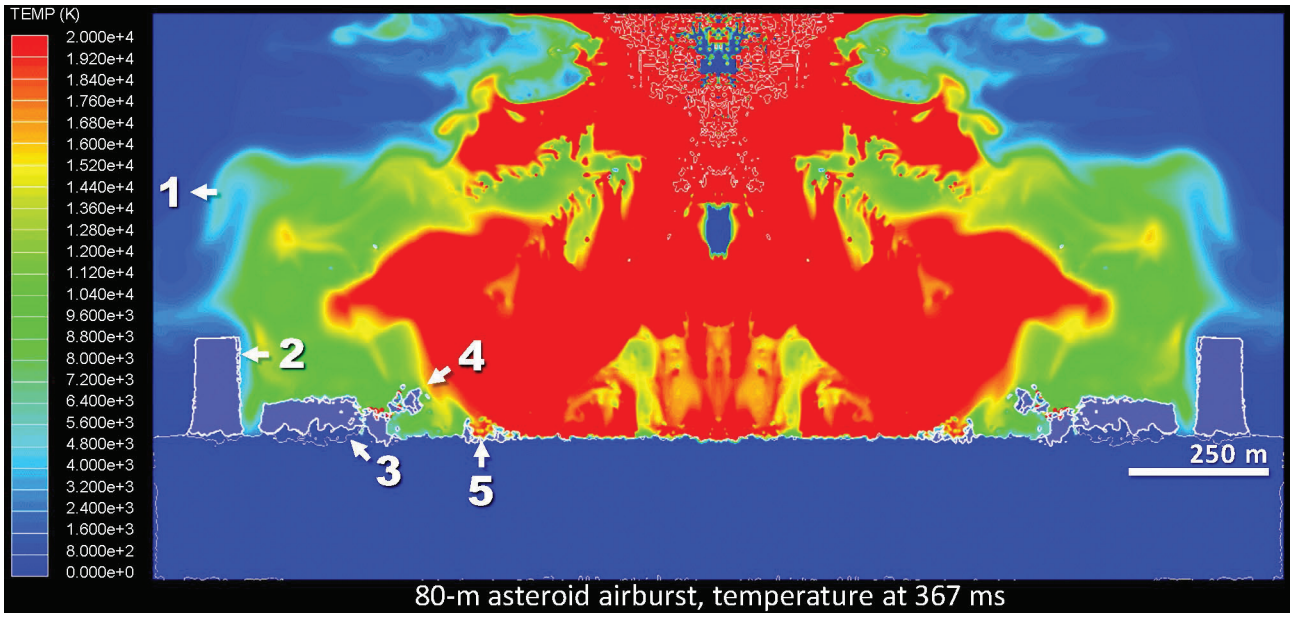


Figure 11: 80-m asteroid, semiquantitative temperature (shows convection currents) at 367 ms. The maximum shock speed = <7,000 m/s, and the maximum pressure decreases to ~8 GPa, sufficient to produce shock metamorphism. The estimated maximum temperature is ≥95,000 K, based on the existing literature [99]. **#1)** The asteroid airburst is >2,000 m wide. **#2)** The temperature at the surface of the high-rise building is sufficient to vaporize most materials. **#3)** The high-velocity, high-pressure wave severely damages the tallest building. **#4)** The high-velocity, high-pressure wave has demolished the smallest building and ejected most of its debris upwards. **#5)** The temperatures in some surface craters briefly exceed the melting point of quartz, producing meltglass.

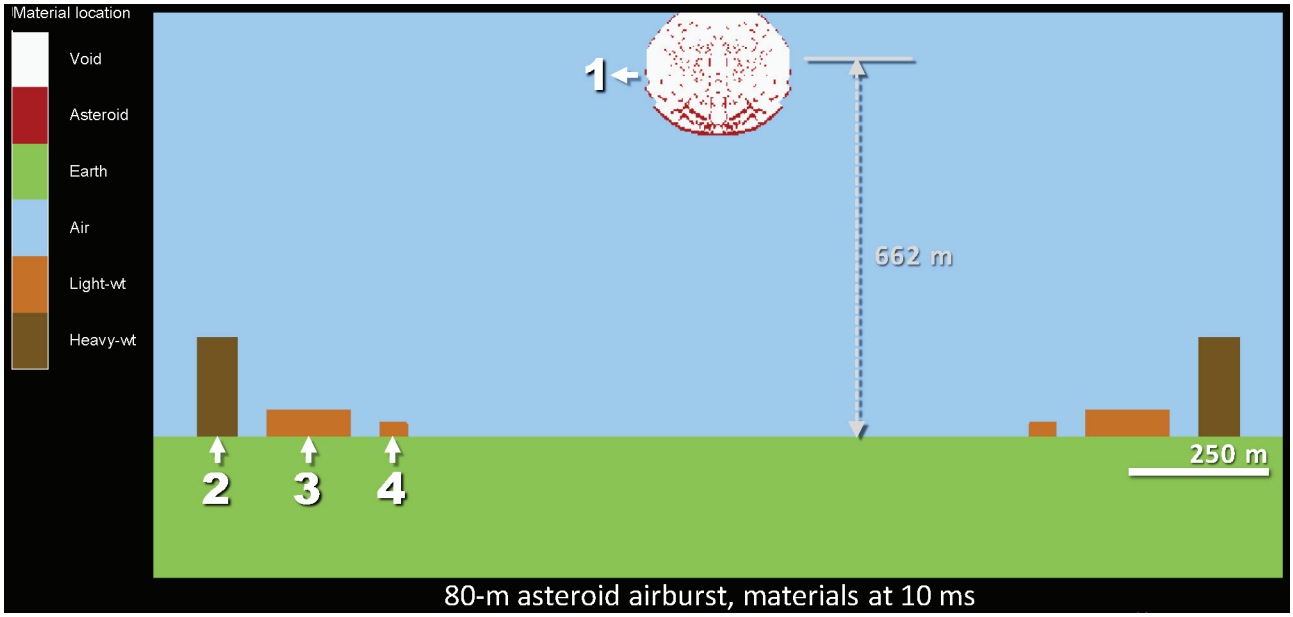


Figure 12: 80-m asteroid, visible state of materials at 10 ms. **#1)** The airburst is ~265 m wide at an altitude of 662 m. Bolide fragments (red) expand outward, creating near-vacuum conditions (white, "void"), through which asteroid fragments travel faster because of the lack of atmospheric friction. Shock speed at 10 ms is 23,000 m/s, pressure = 130 GPa in the airburst, and the approximate temperature = 38,000 K. **#2)** The model of a high-strength high-rise building is 75 × 175 m high with a density of ~3.3 g/cm^3. **#3)** Model of a large, low-strength building is 50 × 150 m long at ~1.6 g/cm^3. **#4)** Model of a small, low-strength building is 25 × 50 m long at ~1.6 g/cm^3. The field of view is 2000 × 1000 m.

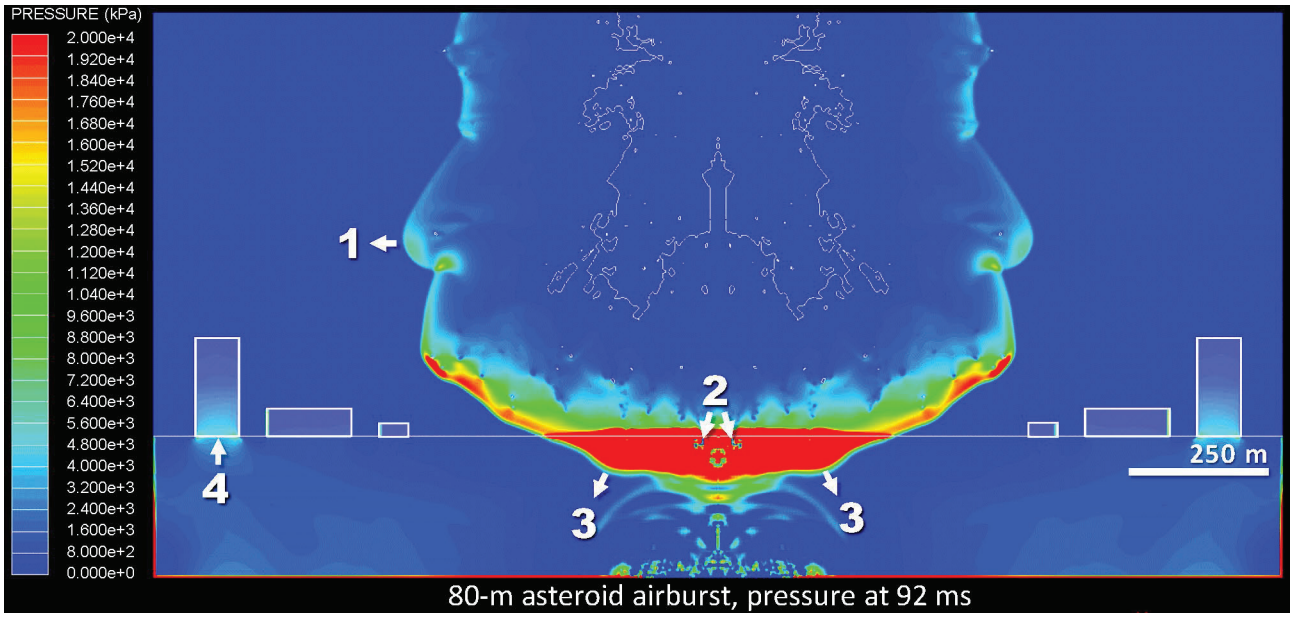


Figure 13: 80-m asteroid, pressure at 92 ms. **#1)** The asteroid airburst is ~1100 m wide, maximum shock speed = 7400 m/s, and the approximate maximum temperature is estimated as ≥95,000 K, based on the existing literature [99]. **#2)** The high-velocity, high-temperature, high-pressure wave melts surface sediment, and impactor fragments create shallow craters. **#3)** High-pressure fragments strike the Earth at 15 GPa in small areas, sufficient to produce shock metamorphism. **#4)** As the lateral pressure increases on the high-rise building, it produces added strain at the base of the building.

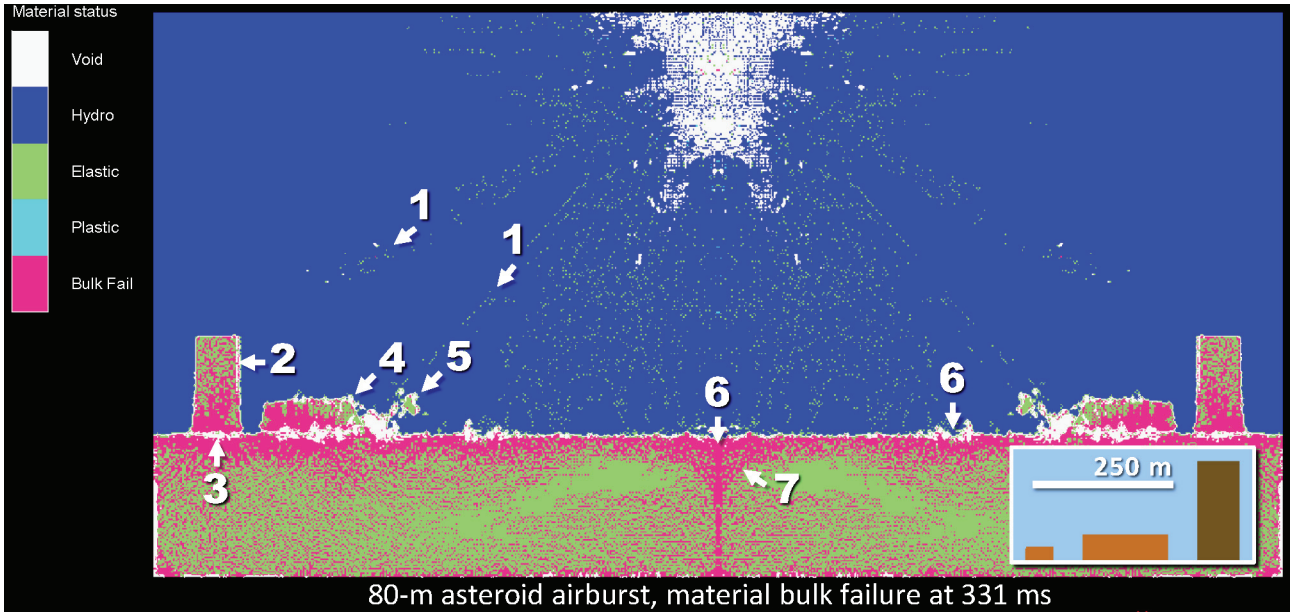


Figure 14: 80-m asteroid, bulk failure at 331 ms. **#1)** The airburst is >2000 m wide. **#2)** The high-rise building shows extensive surface and interior damage but remains standing. The bottom right inset shows original building shapes and sizes. **#3)** The pressure wave damages the building-earth interface, melting and vaporizing some material (white). **#4)** The medium-sized building is heavily damaged, and some material has been ejected upwards. **#5)** The small building suffers more extensive damage. Asteroid fragments travel faster through the near-vacuum zone (white), so they are capable of greater damage. **#6)** Fragments create multiple shallow craters up to ~5 m deep and spanning ~1,480 m. Surface materials melt and mix with impactor vapor and fragments, reported to be less than ~2 wt% [87, 147, 148]. **#7)** Earth's surface is damaged beyond its shear strength (called bulk failure, shown in red) and becomes pulverized or amorphized (Autodyn does not determine its exact state). Bulk failure occurs at the ground impact points and as the pressure wave expands into the Earth. During the first 200 ms, maximum shock speed = 30,000 m/s; maximum semiquantitative temperature = ≥95,000 K; and maximum pressure = >200 GPa. ***Click the bar below for the Bulk Failure video.***

Click for Video: 80-m, Bulk Failure

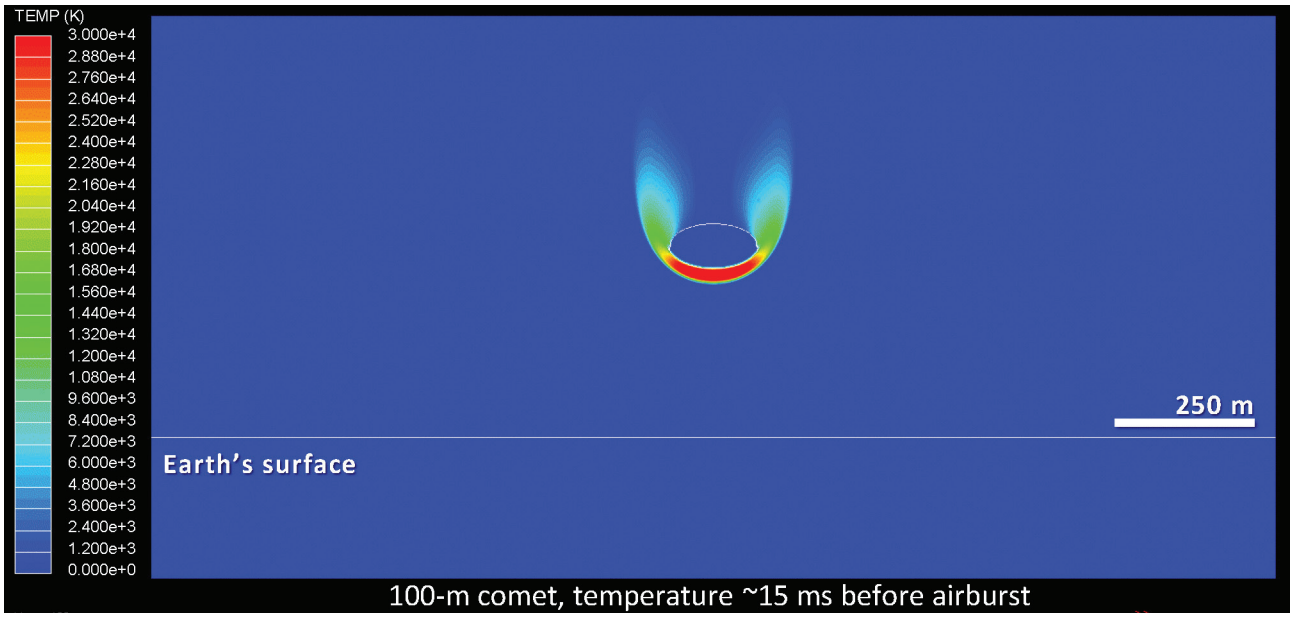


Figure 15: 100-m comet, semiquantitative temperature (shows convection currents). The comet is modeled as a solid deformed sphere but is assumed to be a swarm of co-moving fragments and vapor. Approximately 15 ms before the airburst, when the bolide is ~350 m above the surface, atmospheric friction causes the impactor to deform into a pancake-like shape, although the airburst energy is the same whether or not the object is fragmented. Velocity is ~8,600 m/s, the trail is ~300 m wide, the estimated temperature in the shock front and wake of the bolide is ~30,000 K, and the external pressure is ~127,000 kPa (0.127 GPa). Estimated recurrence interval = ~2500 years [40, 42], although this interval applies to all 100-m impact events, not just airbursts. The field of view is 2000 × 1000 m. ***Click the bar below for the Temperature video.***

Click for Video: 100-m, Temperature

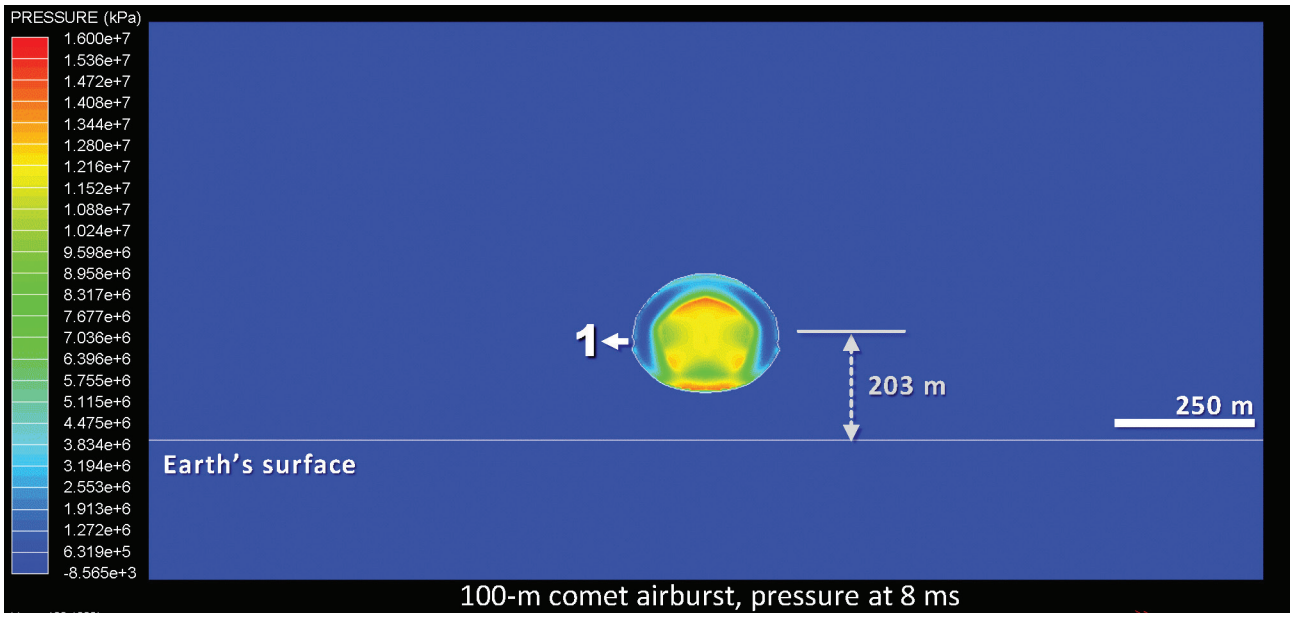


Figure 16: 100-m comet, pressure at 8 ms. **#1)** The touch-down airburst is ~275 m wide at an altitude of 203 m. Maximum internal pressure = 16 GPa, shock speed = 50,000 m/s, and maximum estimated temperature = 45,000 K. ***Click the bar below for the Pressure video.***

Click for Video: 100-m, Pressure

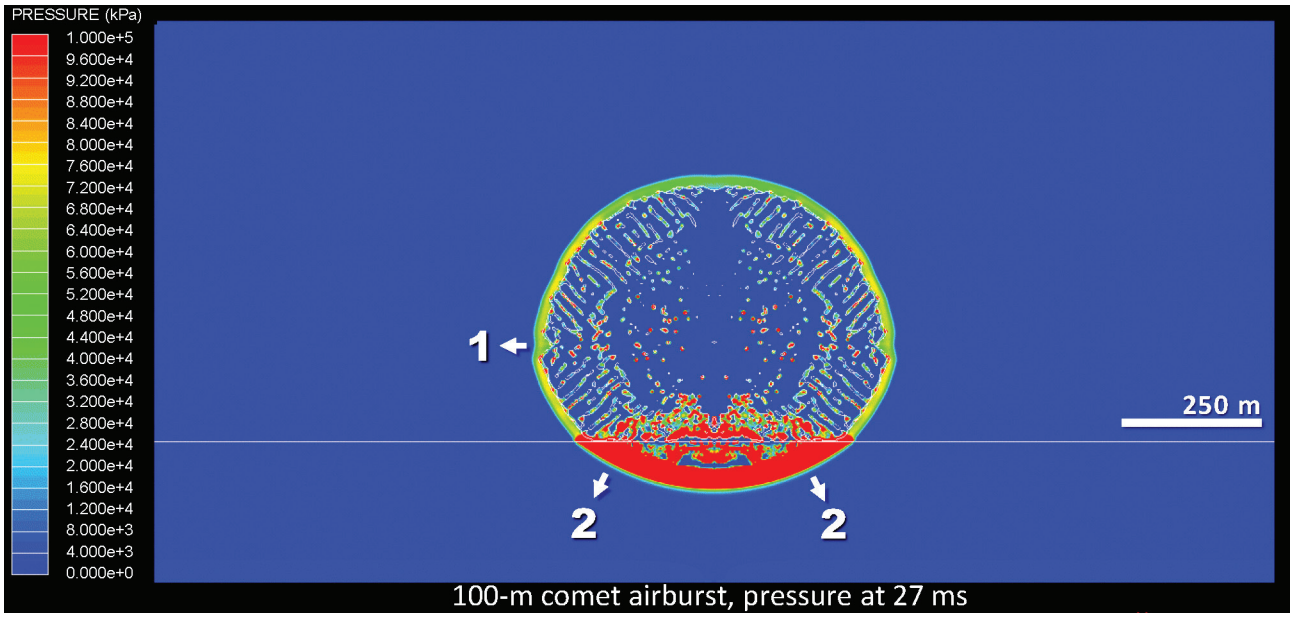


Figure 17: 100-m comet, pressure at 27 ms. **#1)** The comet airburst is ~660 m wide. The maximum shock speed = 100,000 m/s, and the maximum temperature is estimated at ≥95,000 K, based on existing literature [99]. **#2)** High-pressure fragments strike the surface at 6 GPa, sufficient to produce shock-fractured quartz.

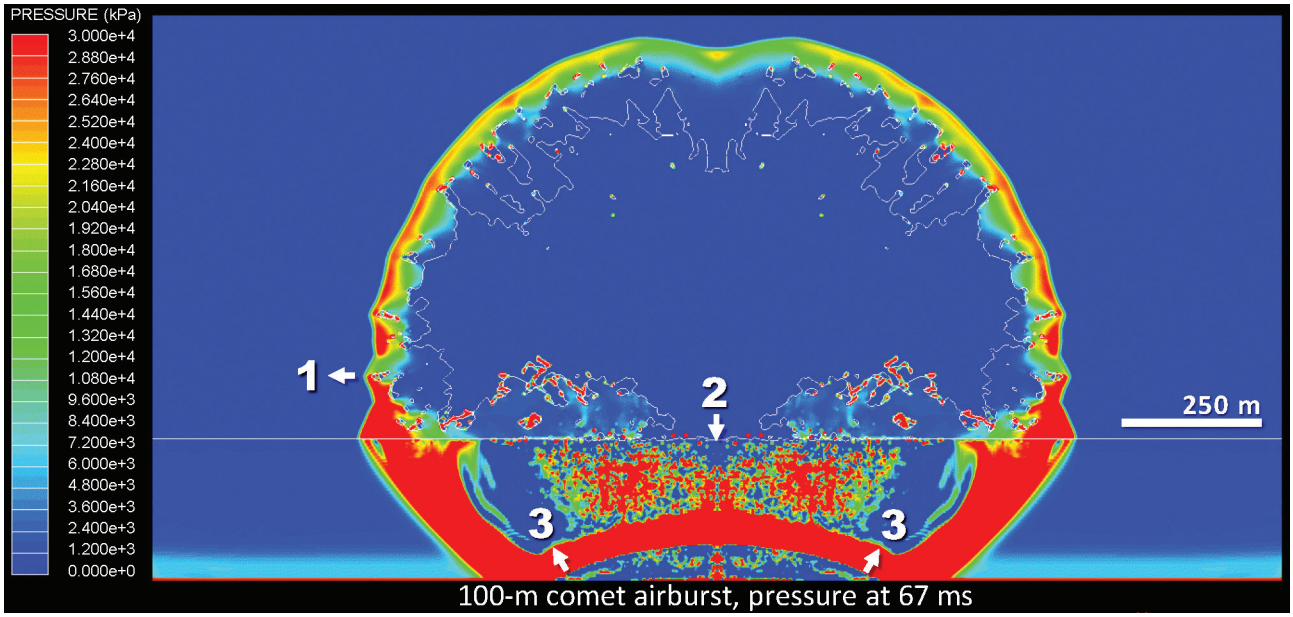


Figure 18: 100-m comet, pressure at 67 ms. **#1)** The comet airburst is ~1275 m wide. Maximum shock speed = 92,000 m/s, and maximum temperature is estimated as ≥95,000 K, based on the existing literature [99]. **#2)** Comet fragments strike the Earth, producing craters and surface damage. **#3)** A high-pressure reflection wave (~5 GPa) rebounds upward off a dense bedrock layer. This pressure is sufficient to produce shock metamorphism.

shock metamorphism in quartz [73]. Previous studies also report that the Trinity nuclear airburst produced shock-fractured quartz [73, 75, 76]. The modeled and actual pressure ranges are the same (Table 5).

Shock speed The Trinity shockwave was ~185 m wide after 62 ms for a velocity of ~2985 m/s [80]. The modeled value for Trinity of 1280 m/s at 64 ms when the fireball was ~82 m wide is ~2.3× smaller in diameter (Table 5).

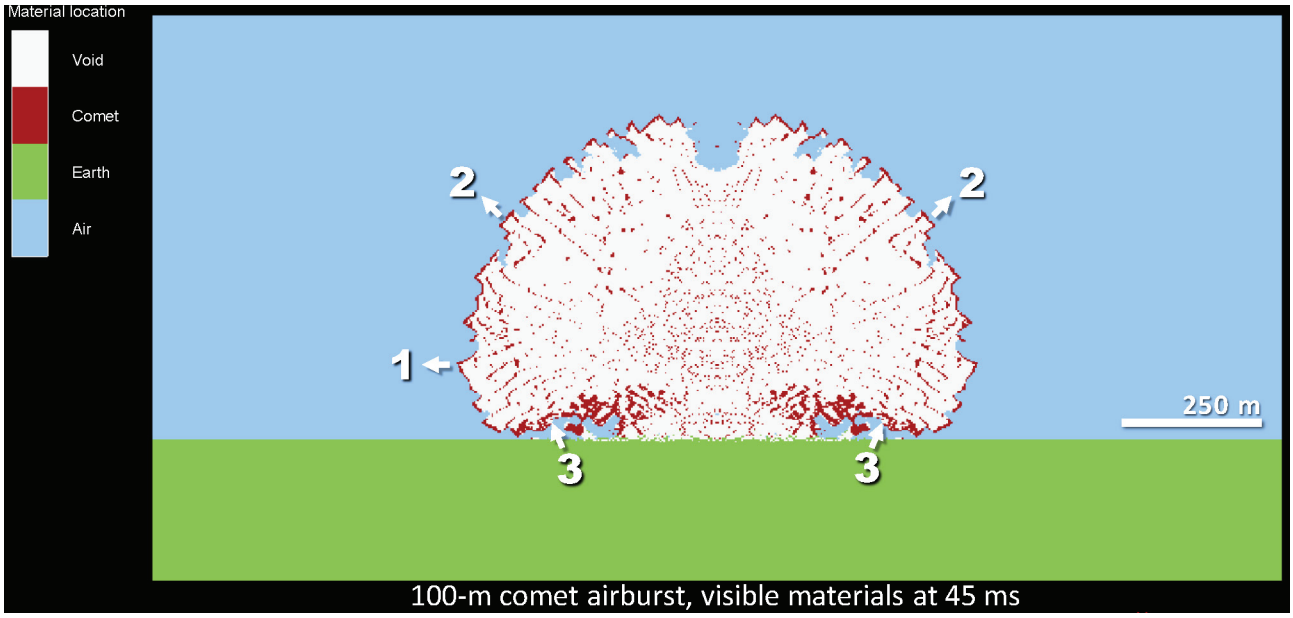


Figure 19: 100-m comet, visible representation at 45 ms. **#1)** The comet airburst is ~920 m wide. Maximum shock speed = 90,000 m/s, and maximum temperature is estimated as ≥95,000 K, based on the existing literature [99]. **#2)** Comet fragments (red) expand up and outward from the airburst's center. Comet fragments travel faster through a near-vacuum (white). **#3)** A high-pressure wave (~1.6 GPa) of comet fragments (red) rebounds upward as a reflection wave. This pressure is sufficient to produce shock metamorphism.

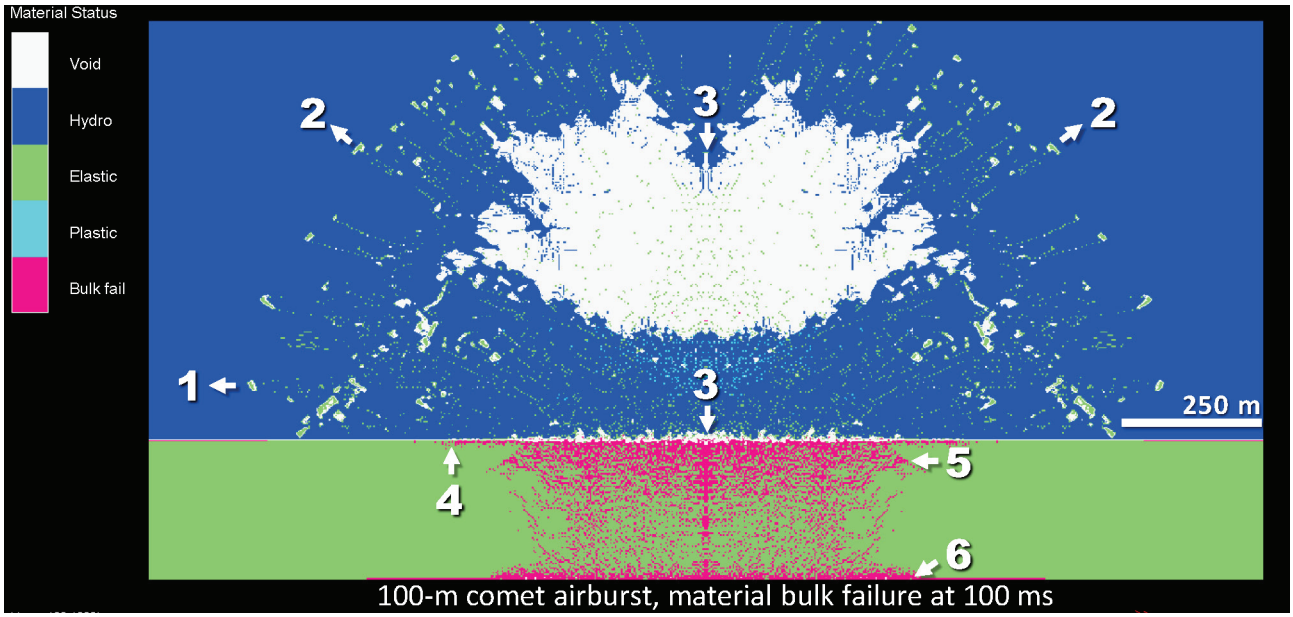


Figure 20: 100-m comet, bulk failure at 100 ms. **#1)** The comet airburst is ~1645 m wide. Maximum shock speed = 93,000 m/s, and the maximum temperature is estimated as ≥95,000 K, based on the existing literature [99]. The maximum pressure = 1.5 GPa, sufficient to produce shock metamorphism. **#2)** Comet fragments (green) expand outward from the airburst. **#3)** A near-vacuum zone (white) is produced in the center of the airburst and at some places on the ground surface. Comet fragments travel faster through the near-vacuum zone, so they are capable of greater damage. **#4)** Comet fragments strike the Earth, producing shallow craters up to 10 m deep, spanning 920 m. **#5)** Earth's surface is heavily damaged (bulk failure) beyond its shear strength, becoming pulverized or amorphized (red). **#6)** Increased bulk failure occurs when the pressure wave encounters a dense bedrock layer.

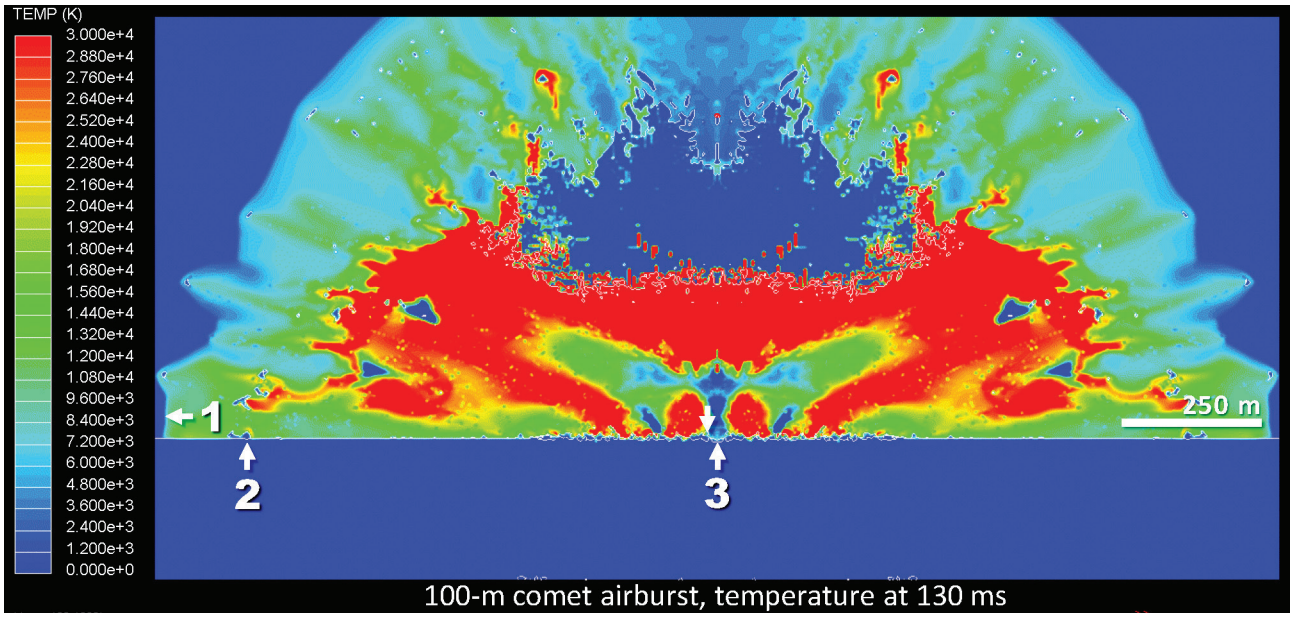


Figure 21: 100-m comet, semiquantitative temperature (shows convection currents) at 130 ms. **#1)** The comet airburst is ~2000 m wide. Maximum shock speed = 92,000 m/s; maximum pressure = 1.5 GPa, sufficient to produce shock metamorphism. **#2)** Comet fragments strike the Earth, producing a large group of mini-craters up to 10 m deep, spanning ~1700 m. **#3)** The cratering spans ~700 m at ground zero. During the first 150 ms of the 100-m comet model, the maximum shock speed = 100,000 m/s, and the maximum pressure = >200 GPa.

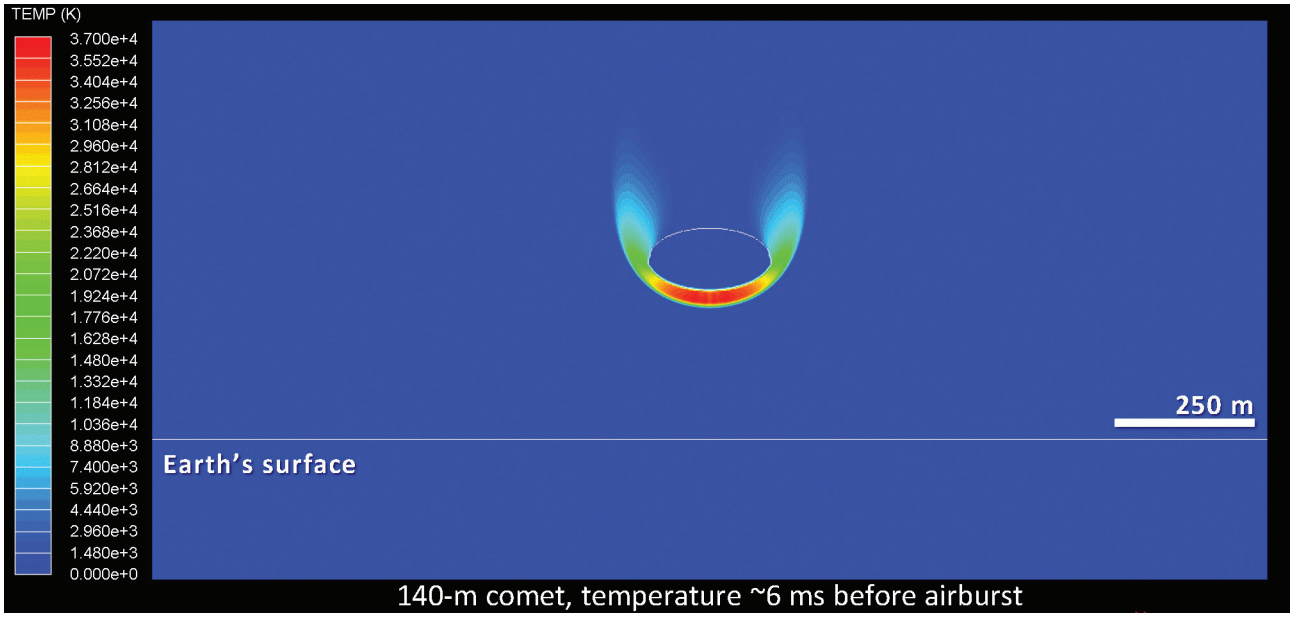


Figure 22: 140-m comet, semiquantitative temperature (shows convection currents). The comet is modeled as a solid deformed sphere, but in actuality, it is assumed to be a swarm of co-moving fragments and vapor. Atmospheric friction causes the swarm to assume a pancake-like shape. Nevertheless, the airburst energy is the same. A few ms before the airburst occurs, the comet is ~350 m above the surface. Object velocity is ~12,000 m/s, the trail is ~350 m wide, the approximate temperature in the shock front is ~37,000 K, and the external pressure is ~110,000 kPa (0.11 GPa). Estimated recurrence interval = ~7400 years [40, 42], although this interval applies to all 140-m impact events, not just airbursts. The field of view is 2000 × 1000 m. ***Click the bar below for the Temperature video.***

Click for Video: 140-m, Temperature

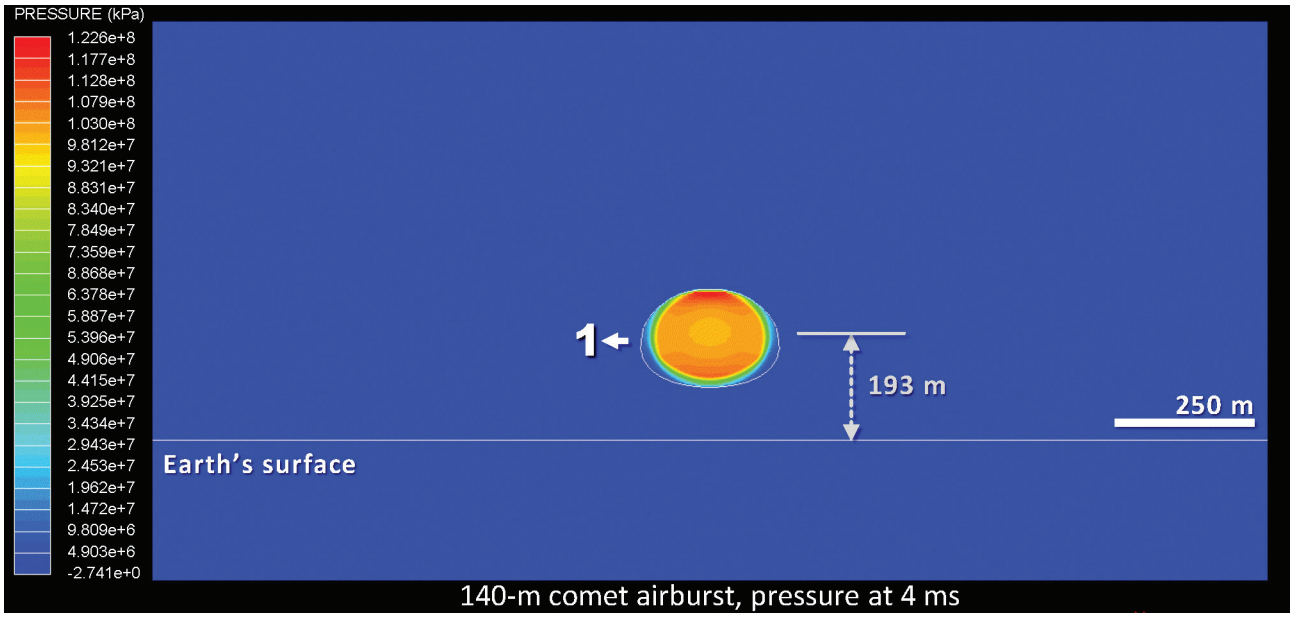


Figure 23: 140-m comet, pressure at 4 ms. **#1)** The touch-down airburst is ~250 m wide at an altitude of 193 m. Maximum internal pressure = 120 GPa, shock speed = 62,000 m/s, and maximum approximate temperature = 66,000 K. ***Click the bar below for the Pressure video.***

Click for Video: 140-m, Pressure

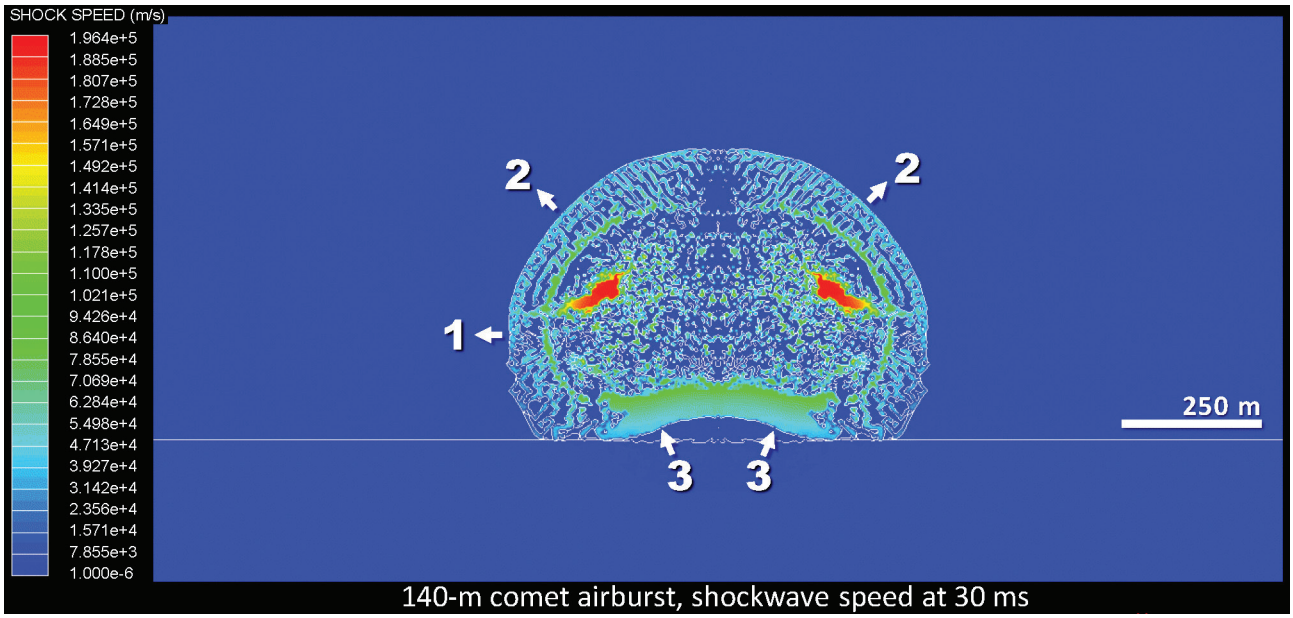


Figure 24: 140-m comet, shockwave speed at 30 ms. **#1)** The airburst is ~740 m wide. Maximum internal pressure = 6.5 GPa and the approximate maximum temperature = ≥95,000 K, based on the previous literature [99]. **#2)** Comet fragments expand at ~200,000 m/s. **#3)** An upward-moving reflection wave forms as comet fragments and vapor rebound off Earth's surface.

Temperature Although it was impossible to model accurate temperatures in this study, some experimental data exist. For Trinity, Glasstone and Dolan [81] (their Fig. 2.123) estimated the maximum temperature as ~300,000 °C, and Brode [82] reported that temperatures at the center of an atomic fireball can reach ~700,000 K. Both of these temperatures fall within the range modeled by Autodyn (Table 5).

Regardless of the limitations in determining temperatures in the Trinity fireball, the reported and modeled temperatures

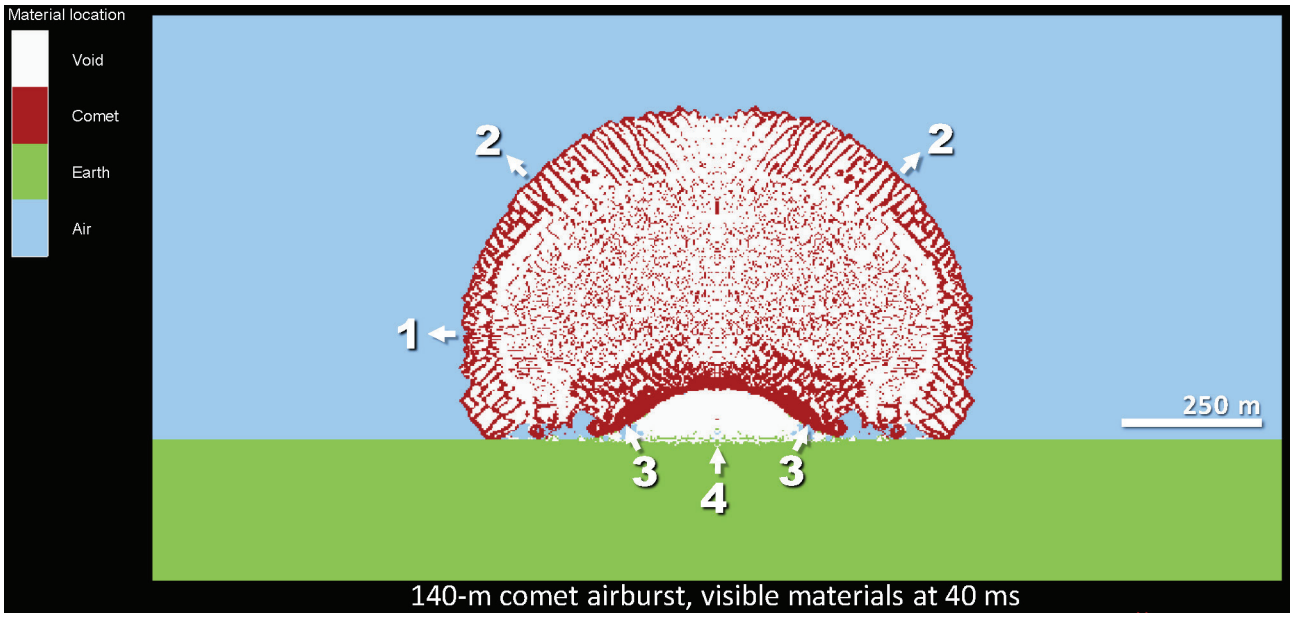


Figure 25: 140-m comet, visible materials at 40 ms. **#1)** The airburst is ~915 m wide. Maximum internal pressure = 5.1 GPa, and the approximate maximum temperature is ≥95,000 K, based on the previous literature [99]. **#2)** Comet fragments expand at ~160,000 m/s. Comet fragments travel faster through the near-vacuum zone (white), so they are capable of greater damage. **#3)** A reflection wave forms as comet fragments rebound off Earth's surface, creating a near-vacuum zone. **#4)** Comet fragments damage Earth's surface, creating craters up to 10 m deep. ***Click the bar below for the Visible Materials video.***

Click for Video: 140-m, Visible Materials

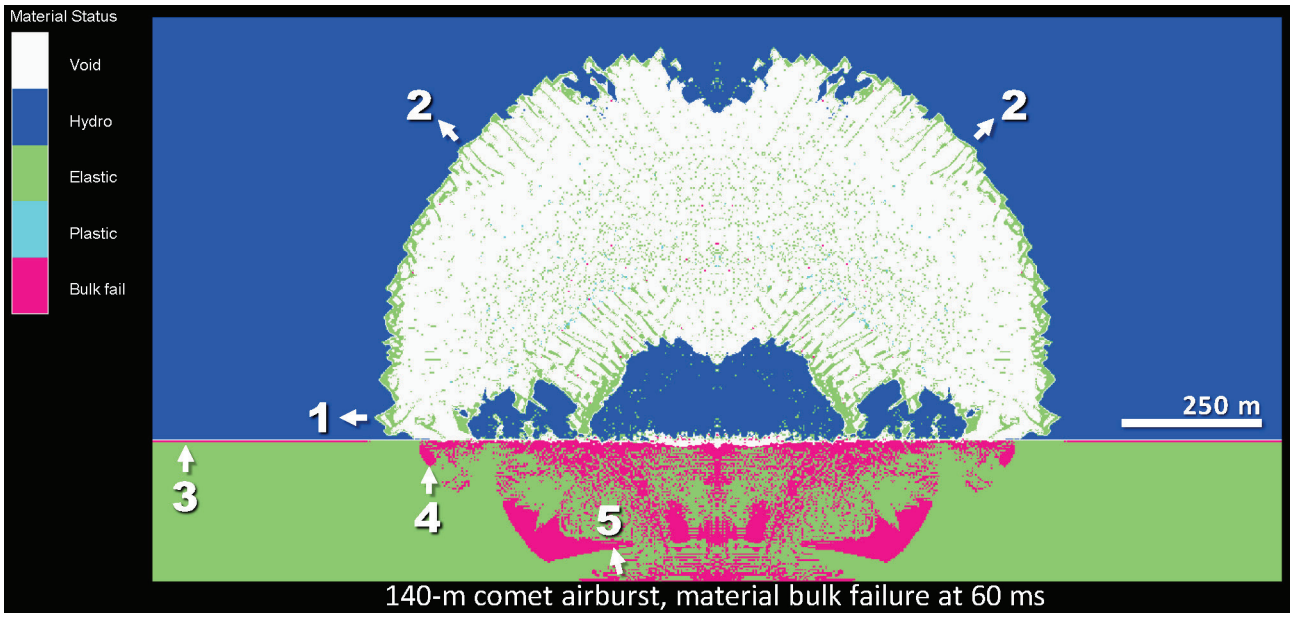


Figure 26: 140-m comet, material bulk failure at 60 ms. **#1)** The airburst is ~1190 m wide. Maximum internal pressure = 4.7 GPa, and the approximate maximum temperature is ≥95,000 K, based on the previous literature [99]. **#2)** Comet fragments (green in airburst) expand at ~140,000 m/s. A near-vacuum zone (white) is produced in the center of the airburst and at the ground surface. Comet fragments (green) travel faster through the near-vacuum zone, so they are capable of greater damage. **#3)** Earth's surface is heavily damaged (bulk failure), becoming pulverized or amorphized (red). **#4)** Comet fragments strike Earth's surface, creating numerous shallow craters up to 10 m deep, collectively spanning 1000 m. **#5)** Additional bulk failure occurs when the pressure wave encounters a dense bedrock layer and reflects upward.

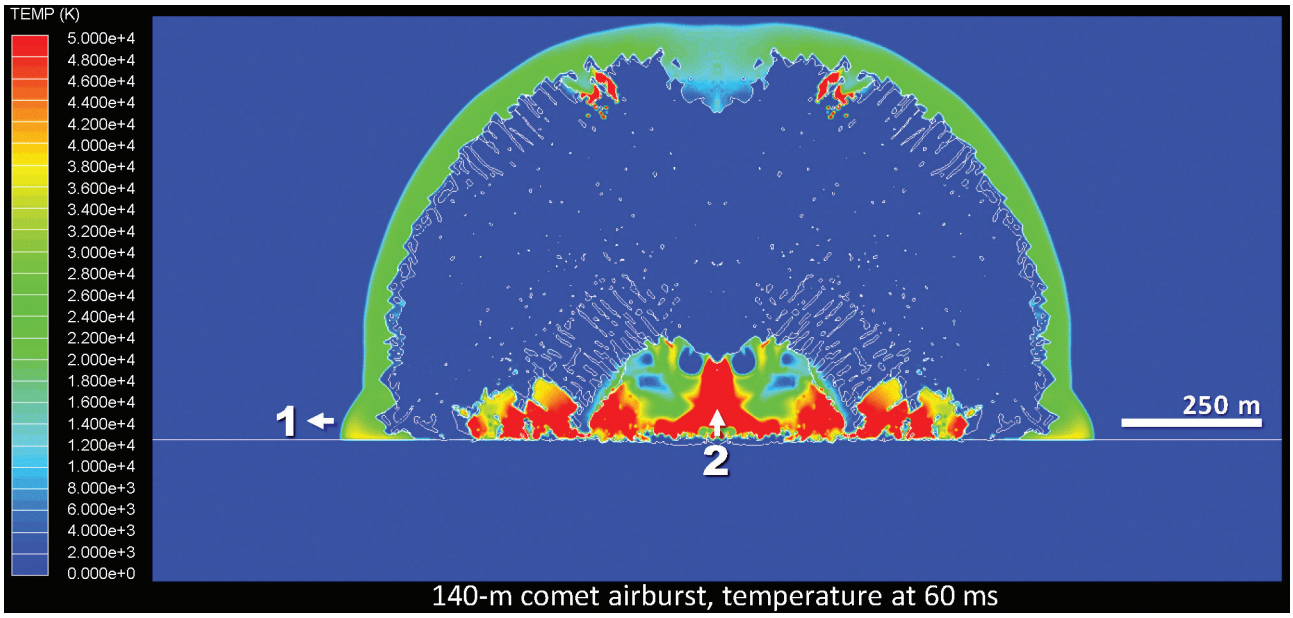


Figure 27: 140-m comet, semiquantitative temperature (shows convection currents) at 60 ms. **#1)** The airburst is ~1190 m wide. Maximum internal pressure = 4.7 GPa. **#2)** The approximate maximum temperature is ≥95,000 K, based on the previous literature [99]. These high temperatures occur at the ground surface near the fragment-generated impact craters and are sufficient to vaporize quartz. Maximum shock speed is 140,000 m/s.

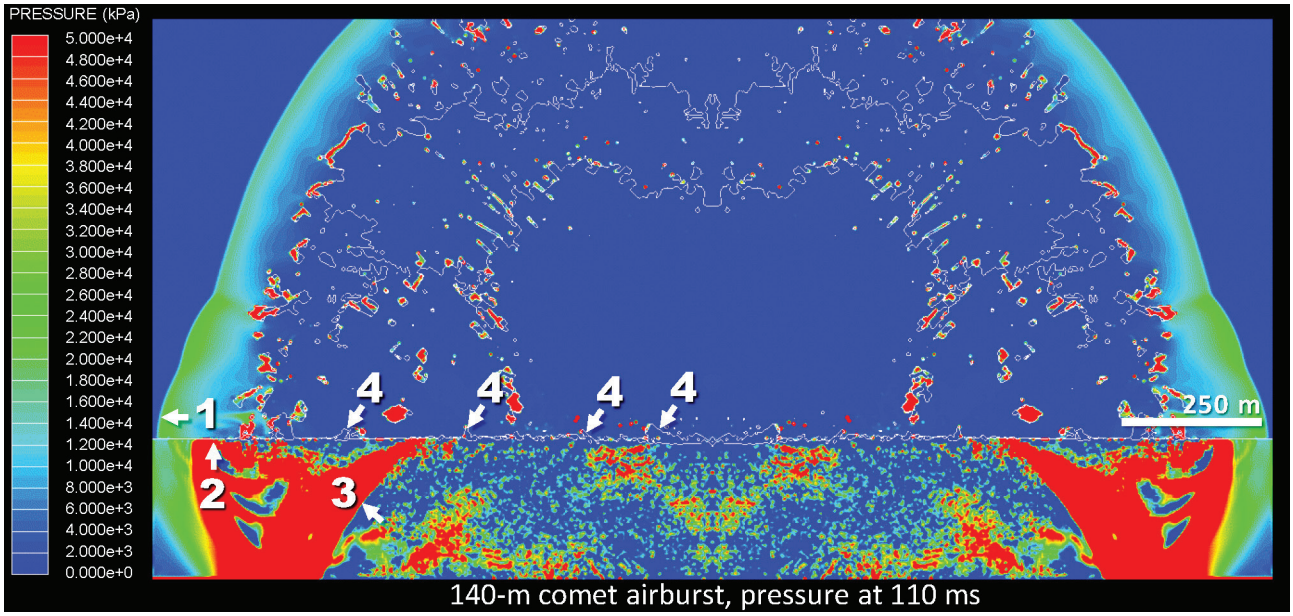


Figure 28: 140-m comet, pressure at 110 ms. **#1)** The airburst is ~2000 m wide. The approximate maximum temperature is estimated at ≥95,000 K, based on the existing literature [99]. Maximum shock speed has decreased to 110,000 m/s. **#2)** The collective crater field is up to 10 m deep and ~1770 m wide. **#3)** A high-pressure reflection wave (>1 GPa) rebounds from bedrock and is sufficient to produce shock metamorphism. **#4)** Fragment impacts and high-velocity shock speed eject melted sediment from the surface. During the first 150 ms of the 140-m comet model, maximum pressure = >200 GPa; maximum shock speed = 87,000 m/s; and maximum temperature is estimated as ≥95,000 K, based on the existing literature [99].

are much higher than the vaporization temperature of quartz at 2230 to 5,000 °C [83, 84]. However, after ~2 s, the fireball temperature abruptly fell below the boiling point of quartz at 2230 °C (Fig. 2.123 in Glasstone and Dolan [81]). We speculate that these highly transitory, extreme temperatures are sufficient to melt the surfaces of quartz grains but are unlikely to melt large grains entirely because of quartz's efficient insulating properties.

Table 3: Summary of modeled parameters.

Trinity, modeled					
Time (ms)	Diam. (m)	Expans. km/s	Press. (GPa)	Temp. (K)	Speed (km/s)
3	16	5.3	60	4.0E+03	25
34	55	1.6	17	3.0E+05	4.6
64	82	1.3	15	3.0E+05	4.6
74	92	1.2	10	3.0E+05	4.5
123	127	1.0	8	3.0E+05	4.3
250	235	0.9	5	3.0E+05	4.2

Asteroid, 80-m					
Time (ms)	Diam. (m)	Expans. km/s	Press. (GPa)	Temp. (K)	Speed (km/s)
3	135	45	>200	2.0E+04	30
10	265	27	130	3.8E+04	23
38	680	18	2	3.2E+04	13
92	1100	12	15	9.5E+04	7.4
116	1220	11	15	9.5E+04	7.4
331	>2000	6	1	9.5E+04	7
367	>2000	5	8	9.5E+04	7

Comet, 100-m					
Time (ms)	Diam. (m)	Expans. km/s	Press. (GPa)	Temp. (K)	Speed (km/s)
8	275	34	17	4.5E+04	50
27	660	24	6	9.5E+04	100
45	920	20	1.6	9.5E+04	90
67	1275	19	5	9.5E+04	92
100	1645	16	1.5	9.5E+04	93
130	>2000	15	1.5	9.5E+04	92

Comet, 140-m					
Time (ms)	Diam. (m)	Expans. km/s	Press. (GPa)	Temp. (K)	Speed (km/s)
4	250	63	120	6.6E+04	62
30	740	25	6.5	9.5E+04	200
40	915	23	5.1	9.5E+04	160
60	1190	20	4.7	9.5E+04	140
110	>2000	18	1	9.5E+04	110

Values calculated by Autodyn for the four models. "Expans" represents the modeled expansion rate in km/s of the visible fireball; "Speed" represents the modeled expansion rate in km/s of the shockwave.

Kieffer [85] analyzed shock-metamorphosed sandstone from Meteor Crater and concluded that the shock metamorphism of quartz commenced at 5.5 GPa, well below the pressures determined for Trinity. Later, Kieffer et al. [86] reported quartz grains from Meteor Crater that they considered had been shocked at <10 GPa to form shock fractures infilled with amorphous silica. To explain this, they proposed a process called "jetting," in which molten quartz is injected under high pressure into shock-generated fractures in the grains. Wakita et al. [87] also observed that during the early stages of an impact, molten material might be jetted when the impactor contacts target rocks.

In support of jetting, Ernstson [88, 89] conducted laboratory experiments and field observations of touch-down airbursts in Germany and the Czech Republic. He found that rocks and grains may fracture due to thermal shock and spallation, during which the stress on the target materials exceeds their tensile strength. If the shock pressures are sufficient to melt or vaporize the target material, silica vapor or melt can be injected into the fractures.

This mix of melted material usually contains <1 wt% of the impactor [90], typically containing high levels of elements such as Ni, Co, Pt, and Ir. Impact jetting has also been proposed to produce melt in lightly shocked material during grain-on-grain collisions in the terrestrial target material [87]. The jetting hypothesis is consistent with observations from the Trinity nuclear detonation and should also apply to touch-down airbursts by asteroids and comets.

Table 5 shows that most measured Trinity parameters (temperature, pressure, shock speed, and fireball expansion) are reasonably similar to the modeled values (differences of ~0.76 to 2.3 times). The Trinity comparison suggests that Autodyn's models are also accurate enough for modeling touch-down airbursts caused by asteroids or comets.

Modeled results for asteroids and comets

Pressure

Autodyn calculated that touch-down airbursts by asteroids and comets could generate ground-surface pressures of up to 28 GPa. This result raises the question of the lower pressure limit required to produce shocked quartz. To address this, Christie et al. [91] performed laboratory experiments to generate slow-strain conditions in milled quartz cylinders. These experiments used a confining pressure of 1.5 GPa and a stress differential of up to 3.6 GPa to produce glass-filled shock lamellae.

Further laboratory experiments by Kowitz et al. investigated the shock alteration of quartz grains using a steel plate explosively driven at various pressures into cylinders of quartz-rich sandstone [92–94]. Visible shock fractures infilled with amorphous silica began to form at ~2.5 to 5 GPa [92, 93] as glass-filled "sub-planar, intra-granular fractures [93]." These experiments indicate that glass-filled shock-generated features may form in quartz even at pressures well below those modeled by Autodyn.

Shock speed

Autodyn calculated 6300–200,000 m/s surface shock speeds for asteroids and comets. Multiple experiments support such high velocities. Stöffler et al. [95] performed experiments using NASA's vertical gun to fire 0.3-g cylindrical

Table 4: Modeling variations.

Bolide Type	Entry Angle (°)	Diam. (m)	Energy (Mt)	Burst ht. (m)	Density (kg/m^3)	Velocity (km/s)	Breakup ht. (km)	Frags. hit Earth
Burst height = 600 >< 700 m.								
Asteroid, stony	90	80	13.7	662	1500	17	72.5	Yes
Asteroid, stony	60	92.5	21.2	641	1500	17	72.5	Yes
Asteroid, stony	45	113	38.7	681	1500	17	72.5	Yes
Asteroid, stony	30	160	110	662	1500	17	72.5	Yes
Asteroid, stony	15	310	799	616	1500	17	72.5	Yes
Asteroid, stony	45	80	13.3	6130	1500	17	72.2	Yes
Burst height = 200 >< 300 m.								
Comet, reg. dens.	90	100	57.9	203	1032	30	89.2	Yes
Comet, reg. dens.	60	115	88	268	1032	30	89.2	Yes
Comet, reg. dens.	45	141	162	250	1032	30	89.2	Yes
Comet, reg. dens.	30	200	463	203	1032	30	89.2	Yes
Comet, reg. dens.	15	385	3300	259	1032	30	89.2	Yes
Comet, reg. dens.	45	100	57	5720	1032	30	89.2	Yes
Burst height = 100 >< 200 m.								
Comet, low dens.	90	140	236	193	530	51	108	Yes
Comet, low dens.	60	162	366	159	530	51	108	Yes
Comet, low dens.	45	198	669	192	530	51	108	Yes
Comet, low dens.	30	280	1890	193	530	51	108	Yes
Comet, low dens.	15	541	13600	191	530	51	108	Yes
Comet, low dens.	45	140	13600	5730	530	51	108	Yes

Parameters for the three models (stony asteroids, regular-density comets, and low-density comets) in this study are highlighted in green. Values in red fonts represent changes from the original parameters. While keeping the same approximate burst heights, density, and entry velocity for each model (non-highlighted examples), we varied the entry angles (90°, 60°, 45°, 30°, and 15°). Corresponding changes in diameter and energy (Mt) are shown. For the blue highlighted examples, we kept diameters, densities, and velocities the same while changing the entry angle to 45°. This change increased the burst heights to ~6 km for all three types of bolides so that these events no longer touched down and, instead, became high-altitude airbursts.

Table 5: Trinity, comparison of actual to modeled values.

Trinity	Autodyn values	Actual values	Factor	Source
Pressure, minerals	5-60 GPa	5-60 GPa	=	Hermes et al., 2023
Pressure, ground	0.10 GPa @ 63 m	0.076 GPa @ 63 m	0.76×	Marley et al., 1946
Temperature	>300,000 K	~300,000 K	≈	Glasstone & Dolan, 1977
Shock speed, 62 ms	1280 m/s	2985 m/s	2.3×	Taylor, 1950
Fireball diameter	82 m @ 64 ms	185 m @ 62 ms	2.3×	Taylor, 1950
Crater width	75 m	80 m	≈	Glasstone & Dolan, 1977

We compared the Autodyn calculated values with known or estimated values for the Trinity nuclear airburst. Of six key parameters, three modeled values were equal to actual values, and three differed from actual values by ~0.76–2.3 times, a reasonably similar comparison.

Lexan projectiles vertically into quartz sand at 5.9 to 6.9 km/s, well within the range generated in Autodyn's models. These experiments produced shock-metamorphosed quartz particles.

Ebert et al. [96] used a small sphere of meteoritic material weighing 4.12 g and fired at ~4.56 km/s into sandstone. The ejecta fragments included shock-metamorphosed quartz grains, fully melted quartz grains, and melted sandstone, as predicted for small impactor fragments in our study.

Similarly, Boslough et al. [97] used NASA's vertical gun to demonstrate that 32-mm-diameter impactors can produce shocked quartz. They fired spherical impactors at 4.61 km/s into unconsolidated quartz and 4.97 km/s into a sandstone block. They reported that both experiments produced significant shock metamorphism at lower velocities than the modeled airbursts reported here.

Wünnemann et al. [98] also used NASA's vertical gun for experiments with small projectiles consisting of Lexan cylinders (1.2 g/cm^3) and aluminum spheres (2.8 g/cm^3) fired vertically into quartz sand with velocities ranging from 5.86 to 6.90 km/s. These experiments also employed the iSALE-2D hydrocode and found excellent agreement between the experiments and their models. Three types of impact-related particles were formed: (i) melted particles, i.e., meltglass, (ii) shock-lithified aggregates, and (iii) shock-metamorphosed grains. In addition, shocked quartz and meltglass were produced at velocities well below those modeled here by Autodyn for touch-down airbursts.

Temperature

Multiple other models and observations support the extreme temperature range for the touch-down airburst models presented here. Even for modeled high-velocity (35 km/s) 10-cm-wide meteoroids, far smaller than the bolides modeled here, Silber et al. [99] reported meteoroid temperatures ranging up to 95,000 K, both in the shock front and in the wake of the meteoroid. Also, Zhilyaev et al. [100] reported that, although there are no direct measurements of temperatures associated with a meteor trail, a model of a small 1-cm meteoroid suggested temperatures of up to 100,000 K. In the current study, Autodyn modeled estimated temperatures >95,000 K. However, these values are considered semiquantitative, so ~95,000 K from the literature is adopted here.

Proposed past touch-down airbursts

The following are crater-forming airbursts, mostly spanning the late Pleistocene through the Holocene. Nearly all examples are proposed as low-altitude Type 2 touch-down airbursts that caused extensive damage to Earth's surface, including forming shallow craters filled with meltglass, microspherules, and other airburst-related proxies. Although airbursts mainly vaporize the incoming bolide, fragments commonly reach Earth's surface, and the kinetic energy of the airburst vapor jet may be high enough to produce shallow craters [6, 7, 101].

The Chrudim/Pardubice strewn field in the Czech Republic is ~135 km long [102, 103]. This proposed Holocene-aged touch-down airburst produced extensive clusters of small craters and widely scattered superficial and near-surface occurrences of meltglass, glass-filled fractured quartz, glass-like carbon, and multiple shock effects in polymictic breccias (planar deformation features (PDFs), diaplectic glass, silica ballen structures, and meltglass).

In Saarland, a state in Germany, a touch-down airburst event produced the approximately Holocene-aged, 15-km-long Nalbach/Saarlouis strewn field, including two primary craters, one 250 m, the other 2.3 km in diameter [104–106]. Both craters feature densely extended surficial occurrences of impactites, such as strongly shocked polymictic breccias (PDFs, diaplectic glass, silica ballen structures, heat-altered (toasted) quartz), impact glasses, meltrocks, and shatter cones.

In the Chiemgau district of southeastern Germany, extensive evidence exists for a significant Holocene-age touch-down airburst event [107–116]. The Chiemgau field is approximately elliptical, covering an area of about 60 km by 30 km (1,800 km^2) and containing more than 100 impact craters ranging in diameter from a few m to 1,300 m. The strewn field displays shocked quartz, feldspar and mica; glass-filled fractured quartz; microspherules; microtektites; meltglass; ballen quartz structures; heat-altered (toasted) quartz; glass-covered cobbles; shock-spallation in cobbles and quartz grains; and shatter cones.

One significant piece of evidence for a Chiemgau impact airburst event is the widespread occurrence of chiemite, a pumice-like new impact rock predominantly consisting of >90 wt% amorphous carbon, which has been reported for the first time anywhere in the Chiemgau strewn field. Chiemite contains diamond and carbynes, which require 2500–4000 °C and several GPa of pressure to form. Fossilized plant cell structures and pseudomorphs of chiemite after wood fragments indicate formation by direct shock transformation of organic material such as wood and peat to high-rank carbon by a touch-down airburst [117].

The Chiemgau event has been dated to ~2900–2600 years ago in the Bronze Age/Celtic Era using a novel impact proxy (artifact-in-impactites), in which culturally datable artifacts are embedded in shocked impact meltrocks [111, 112].

At Tall el-Hammam in Jordan, northeast of the Dead Sea, a touch-down airburst by a 50-m to 75-m bolide has been proposed to have destroyed an ancient city ~3600 years ago [11]. The high-temperature event produced melted pottery and mudbricks, shock-fractured quartz, microspherules, and meltglass. In addition, hypervelocity winds from the airburst were proposed to have laterally distributed potsherds, charred grains, charcoal, and bone fragments in narrow trails up to ~22 m long from SW to NE across the demolished city.

A 50-km-wide touch-down airburst/impact event was proposed for the Niederrhein region in Germany, where there are dozens of small craters (100–200 m wide) [118]. A large mass of stony meteorites, most likely from a rubble-pile basaltic asteroid, has been recovered from 40 locations. In addition, the evidence includes polymictic breccia, diaplectic glass, shock-fractured quartz, shocked feldspar, and highly vesicular meltglass with native iron inclusions. The age of this event is unclear, but it is most likely Holocene in age and no older than the middle Pleistocene.

As discussed above, a large linear strewn field of ~12,500-year-old meltglass has been reported in a 75-km-long narrow corridor of the Atacama Desert in Chile that some have attributed to a low-angle, touch-down airburst [16–18]. The studies reported twisted and folded silicate glasses up to 4 m in diameter and up to 15–25 cm thick [19] that contain meteoritic grains [18] and shocked quartz grains [19]. Boslough et al. [20] attribute the 75-km-long field of meltglass to "*low-altitude airbursts from six fragments of a single 120-m diameter comet* [that] *generated separate airbursts.*"

At the 12,800-year-old Younger Dryas boundary, numerous studies have reported peak abundances of shock-fractured quartz, meltglass, microspherules, soot and charcoal from impact-related biomass burning, and platinum-iridium anomalies [21–23, 26, 65, 119–133]. These unusual materials are suggested to have resulted from multiple hemispheric airbursts, some high-altitude and some as touch-downs, caused by the Earth's collision with dust and fragments in the tail of a comet [129, 134, 135].

In another example of a proposed airburst, Osinski et al. and others [12–14] reported large quantities of meltglass produced ~145,000 years ago at the Dakhleh Oasis in Egypt. The glass deposits were separated by >40 km and spanned ~400 km^2. The strewn field contains melted silica (lechatelierite, which forms at >1700 °C), shock-fractured quartz, and microspherules [12, 15].

Van Ginneken et al. [3, 7] describe two near-surface airbursts in Antarctica, one ~430,000 years old and a second one ~2.3 Myr old, the oldest ever discovered, in which high-pressure, high-velocity, high-temperature jets intersected the surface [3, 136, 137]. In the younger event, the touch-down airburst distributed melted microspherules across a radius of up to ~1400 km (2×10^6 km^2) [136].

The Libyan Desert glass field formed ~29 million years ago extends across ~6500 km^2 of the desert in Egypt [29] and is estimated to contain 1400 tonnes of meltglass [30], microspherules [31, 32], and shocked quartz [33, 34]. Because no crater has been discovered, some have proposed that a low-altitude airburst produced the field [5, 38]. Other studies interpret the presence of shocked quartz [33, 34] as evidence that it could not have been an airburst and that a typical impact crater exists but remains undiscovered. However, based on evidence from nuclear detonations, Hermes et al. [73] suggested that bolide airbursts can produce glass-filled, shock-fractured quartz without requiring a typical crater-forming impact event.

Other proposed Holocene-aged airbursts have been described, including the following: (i) More than a dozen small craters, including one 300 m in diameter, are part of the Holocene-age Lower Franconia strewn field in Germany [138]. (ii) The Pleistocene/Holocene-aged ~25-km-wide Sachsendorf Bay structure is a proposed airburst/impact crater in northeastern Germany [139]. (iii) The Holocene-aged 20-km-diameter Kolesovice airburst crater in the Czech Republic [140]. (iv) In Finland, a 6400-year-old strewn field contains 33 craters up to 100 m diameter [141].

Possible recurrence intervals for airbursts

The recurrence interval of touch-down airbursts is unknown and currently unquantifiable because none have been observed by scientists in the last few hundred years. The online EIEP [39, 40] provides the following approximations with significant uncertainties: an 80-m asteroid impact event with a wide range of parameters (density, entry angle, and velocity) may recur globally every 1700 years; a 100-m comet every 2500 years; and a 140-m comet every 7400 years. However, these estimates are for all impact events, including high-altitude and touch-down airbursts. Thus, touch-down airbursts are less frequent than these intervals suggest.

As discussed in the previous section above, impact researchers have proposed at least eight touch-down airbursts within the last ~11,700 years across Western Europe (2.2 million km^2): (i) Chrudim/Pardubice in the Czech Republic [102, 103], (ii) Nalbach/Saarlouis in Germany [104–106]. (iii) Chiemgau in Germany [107–116, 142], (iv) Niederrhein in Germany [118], (v) Franconia in Germany [138]. (vi) Sachsendorf Bay in Germany [139], (vii) Seven possibly related strewn fields across about half of the Czech Republic [103], and (viii) a 6400-year-old strewn field in Finland [141]. These eight events suggest one touch-down airburst recurrence approximately every 1500 years across Western Europe. However, because so little is known about touch-down airbursts, this estimate has significant uncertainties, and more research is required to determine an accurate recurrence rate.

Potential hazards of airbursts

In July 2023, the near miss of asteroid 2023 NT1, a 30–60 m asteroid, was only discovered two days after it had passed Earth [143, 144]. The closest approach of 2023 NT1 was only about one-quarter of the Earth-Moon distance and had a potential impact energy of 10 Mt [143, 144], >600 times the energy of the Trinity atomic detonation. If this asteroid's orbit had been slightly different, causing it to collide with Earth, it would have been large enough to have produced a significant touch-down airburst. This recent event is a reminder that even smaller objects pose a significant threat to humans and highlights the importance of understanding the magnitude of the threat posed by small, difficult-to-detect bolides that produce touch-down airbursts over a modern city.

Proposed scenario for touch-down airbursts and their potential effects

Several essential points characterize touch-down airbursts compared to typical crater-forming impact events. This comparison is based on both independent evidence cited herein and our experimental Autodyn and EIEP models:

1. Airbursts are far more common than typical crater-forming impact events.
2. Bolides only slightly smaller than those that produce typical impact craters can produce touch-down airbursts.
3. Fragments from many airbursts reach Earth's surface, typically at terminal velocities.
4. Touch-down airbursts can create relatively shallow craters.
5. High temperatures and pressures from airbursts can produce meltglass and melted microspherules, as with typical crater-forming impact events.
6. Surface collisions by airburst fragments can produce shock metamorphism in various minerals and rocks (PDFs, PFs, and glass-filled shock-fractured minerals), along with ballen structures and shatter cones.

Based on the above, we suggest the following scenario for touch-down airbursts and the features they produce. This scenario is similar to but not identical to that proposed by Boslough and Crawford [4].

1. Touch-down or Type 2 airbursts occur at altitudes sufficiently low for the hypervelocity jet to intersect Earth's surface.
2. Within the first few ms, high temperatures produce *in situ* meltglass.
3. Surficial material drawn into the plume produces Si-rich microspherules (mostly from bulk sediment but also from the impactor) and Fe-rich microspherules (mostly from magnetite grains in the bulk sediment but also from Fe in the impactor).
4. Bolide fragments can strike Earth's surface at hypervelocities, producing small, ephemeral craters, often coalescing into one large, shallow crater.
5. Bolide fragments can produce pressures high enough to produce well-known shock effects in multiple minerals but, at reduced pressures, also fracture quartz and other mineral grains through fragment-to-grain, grain-to-grain collisions, and intra-grain spallation.
6. Furthermore, classically shocked quartz grains can form with parallel, planar lamellae.
7. In addition, extreme temperatures can produce thermal shock fractures in quartz without collisions.
8. The high temperatures (≥2,230 K) boil and vaporize some quartz grains and partially vaporize the surfaces of others. Then, low-viscosity quartz liquid and vapor are injected (jetted) into fractures, producing glass-filled, shock-fractured quartz.

Well-studied crater-forming impacts with large single impactors like Meteor Crater are known to have produced abundant meltglass, microspherules, and shock-metamorphosed grains, the latter of which have long been considered an essential diagnostic proxy for confirming an impact event, making shock metamorphism a 'gold standard' for confirmation. However, our modeling results reveal the potential formation of shock-metamorphosed grains during touch-down airbursts, both from the high-temperature, high-pressure shockwave and from hypervelocity bolide fragments that strike the ground. However, metamorphosed grains appear at lower abundances in touch-down airbursts, making such events challenging to identify in the geologic record. In addition, any shallow craters that form can be easily and rapidly eroded. Nevertheless, even comparatively low concentrations of shock-metamorphosed quartz grains should be satisfactory for positively identifying potential touch-down airbursts when coupled with the presence of high-temperature meltglass and microspherules. Furthermore, our study suggests that the presence of shock-metamorphosed grains, meltglass, microspherules, and other impact-related proxies eliminates the previously accepted requirement for an impact crater. Instead, these proxies may have formed in a touch-down airburst.

Conclusions

This study's model of touch-down airbursts by comets and asteroids revealed pressures, temperatures, and shock speeds high enough to produce shock metamorphism, high-temperature meltglass, and microspherules. If these airbursts occur close enough to the Earth's surface, they can produce multiple shallow craters with scaled-down effects comparable to typical crater-forming impacts. However, such shallow airburst craters are likely geologically ephemeral features easily obscured by sedimentation from wind and water. Without a visible crater, these proxies should be useful in identifying candidate sites of previously unrecognized touch-down airbursts. The evidence suggests that such airbursts are geologically more common than typical large crater-forming events. The airburst-generated extreme temperatures, pressures, and wind velocities are potentially highly destructive, suggesting a pressing need for further research.

Acknowledgments

We thank six reviewers who made thoughtful comments to improve the paper. We specifically thank Dr. Gareth Collins for his helpful emails over the years answering questions regarding the use of the Earth Impact Effects Program. We are grateful to Ted Bunch, who contributed substantially to this study but passed away before its publication. We also thank Metin Ozen and Chris Cowan of Ozen Engineering, Inc. for their assistance with Autodyn. We also are grateful to Lucie Smrcinova for her input. We also thank Eugene Jhong, whose generous grants to the University of South Carolina and the University of California, Santa Barbara, helped make this research possible.

Data availability

All supporting data are included in this manuscript.

Author contributions

A.W. and L.C. conceived the project. A.W., M.Y., J.P.K., C.R.M., M.A.L., G.K., and R.E.H. contributed to and wrote parts of the manuscript and Supporting Information. L.C., A.W., and/or M.Y. conceived/directed/conducted modeling and created figures. A.W. produced the videos. All authors reviewed and approved the manuscript.

Funding

During the study, G.K. was partially supported by the Czech Science Foundation (Grant 23-06075S). Eugene Jhong supported this study through generous grants to the University of South Carolina and the University of California, Santa Barbara. The Comet Research Group also provided funding.

Competing Interests

The Comet Research Group (CRG), a 501(c) (3) nonprofit charitable educational and scientific organization, receives donations from the public and the cofounders. Donations were used for modeling expenses. M.A.L., C.R.M., J.P.K., and A.W. volunteer their time as cofounders or directors of CRG. No co-author receives a salary, compensation, stock, or any other financial benefit from CRG, except co-authors A.W. and M.A.L., who benefit from tax deductions for donations to CRG. A.W. is a co-author of "The Cycle of Cosmic Catastrophes," a book related to the Younger Dryas Impact Hypothesis; he donates all proceeds to CRG. All co-authors were involved in the manuscript preparation. Co-authors A.W., M.A.L., and C.R.M. are editors of this journal but have recused themselves from the decision to review and accept this manuscript.

Methods

For this study, three co-authors (L.C., M.Y., and A.W.) were involved in various stages of the modeling, image rendering, and video production. The modeling was performed with the advice and guidance of L.C., an expert Autodyn instructor for Ozen Engineering, Inc. L.C., who recommended Autodyn as appropriate for this study. His recommendation is based on his modeling work for the U.S. Army Futures Command Combat Capabilities Development Center, where he used Autodyn to create various hydrocode models and simulations, including for geological impacts at high strain rates.

First, we modeled the airbursts using the Earth Impact Effects Program (EIEP) by Marcus et al. [42] and Collins et al. [39, 40] We entered projectile diameters, densities, velocities, entry angles, and target densities to determine the estimated burst heights, energies in megatons and joules, peak overpressures, and wind velocities. Results from the EIEP show that for nearly all low-altitude touch-down airburst events, no typical impact craters form, although large fragments may strike Earth's surface. The airburst energies used in the Autodyn calculations approximately correspond to observed values, where known.

Next, we entered the output generated by the EIEP into Autodyn using the following parameters, assumptions, and specifications:

(i) We used Autodyn's two-dimensional Eulerian hydrocode solver.

(ii) Following Saito et al. [50, 51] and Boslough and Crawford [4], we specified a 90° entry angle for simplicity. Although statistically less likely than a 45° entry angle for asteroids, comets from the spherical Oort cloud are equally as likely to impact at 90° as at any other angle.

(iii) We used the Tillotson equation-of-state (EOS), an expression that describes the relationship among pressure, volume, and temperature during high-speed impacts. The Tillotson EOS only approximates the temperatures involved, so the temperature calculations are considered semiquantitative; they are presented here primarily to illustrate convection currents.

(iv) We also used von Mises strength values to predict the yielding or fracturing of materials under complex loading conditions.

(v) The Hydro (Pmin) failure values were used to determine when a material exceeds a specified pressure value in the tensile direction.

(vi) The appropriate physical/mechanical properties for each material are listed in the Supporting Information.

(vii) All materials were assumed to be homogeneous for this study, but asteroids and comets are likely heterogeneous, fractured, and semi-porous.

(viii) The downward pre-burst and post-burst velocity values provided by the EIEP were entered into Autodyn, which used them in its calculations.

(ix) For our Autodyn models, we used horizontal axial symmetry [50, 51], where only half of the domain is modeled, and the other half is duplicated horizontally through symmetry.

(x) The meshes were modeled at 356 × 356 cells, ranging from 0.28 × 0.28 m for Trinity up to 2.8 × 2.8 m for the asteroid and comet models.

(xi) Following Collins et al. [39], we modeled the bolides as solid deformed spheres, but in actuality, they are hypervelocity swarms of co-moving fragments and vapor. Atmospheric friction causes the swarm to assume a pancake-like shape, and most energy dissipates in the air. In these simplified models, we did not consider

fragmentation; however, we did use the same airburst energy calculated by the EIEP.

(xii) Convergence with respect to spatial resolution was not explored because these models are first-order approximations.

(xiii) Unless otherwise specified, computational input and output were in millimeters (mm), milligrams (mg), and milliseconds (ms). See Supporting Information for input parameters.

In Autodyn, each model's simulation run-time was typically 2–4 hours. The image sequence generation for creating videos typically required 5–10 hours for each parameter, e.g., temperature or pressure. All models and figures were created using Autodyn-2D, versions 2023 R1 and 2023 R1 Student (Ansys, Inc.). Videos were created using Camtasia, Version 23.3.3 (Build 49804), 2023. The figures illustrate visible materials, semiquantitative temperature, pressure, shock speed, and material bulk failure on scales with up to 50 colored divisions.

References

[1] Boslough, M. Airburst Modeling. In *First International Workshop on Potentially Hazardous Asteroids Characterization, Atmospheric Entry and Risk Assessment*, 2015.

[2] Boslough, M. Airburst Modeling. In *Handbook of Cosmic Hazards and Planetary Defense*, 2021, pp. 1–24.

[3] Van Ginneken, M.; Harvey, R.P.; Goderis, S.; Artemieva, N.; Boslough, M.; Maeda, R.; Gattacceca, J.; Folco, L.; Yamaguchi, A.; Sonzogni, C.; et al. The Identification of Airbursts in the Past: Insights from the BIT-58 Layer. *Earth Planet. Sci. Lett.* **2024**, *627*, 118562; doi: 10.1016/j.epsl.2023.118562.

[4] Boslough, M.; Crawford, D.A. Low-Altitude Airbursts and the Impact Threat. *Int. J. Impact. Eng.* **2008**, *35*(12), 1441–1448; doi: 10.1016/j.ijimpeng.2008.07.053.

[5] Boslough, M.B.; Crawford, D.A. Low-Altitude Airbursts and the Impact Threat-Final LDRD Report. Sandia National Lab: Albuquerque, NM, USA, 2007.

[6] Artemieva, N.; Shuvalov, V. Atmospheric Shock Waves After Impacts of Cosmic Bodies up to 1000 m in Diameter. *Meteorit. Planet. Sci.* **2019**, *54*(3), 592–608; doi: 10.1111/maps.13229.

[7] van Ginneken, M.; Goderis, S.; Artemieva, N.; Debaille, V.; Decrée, S.; Harvey, R.P.; Huwig, K.A.; Hecht, L.; Yang, S.; Kaufmann, F.E.D.; et al. A Large Meteoritic Event Over Antarctica ca. 430 ka Ago Inferred from Chondritic Spherules from the Sør Rondane Mountains. *Sci. Adv.* **2021**, *7*(14), eabc1008; doi: 10.1126/sciadv.abc1008.

[8] Brown, P.G.; Hildebrand, A.R.; Zolensky, M.E.; Grady, M.; Clayton, R.N.; Mayeda, T.K.; Tagliaferri, E.; Spalding, R.; MacRae, N.D.; Hoffman, E.L.; et al. The Fall, Recovery, Orbit, and Composition of the Tagish Lake Meteorite: A New Type of Carbonaceous Chondrite. *Science*. **2000**, *290*(5490), 320–325; doi: 10.1126/science.290.5490.320.

[9] Brown, P.G.; ReVelle, D.O.; Tagliaferri, E.; Hildebrand, A.R. An Entry Model for the Tagish Lake Fireball Using Seismic, Satellite and Infrasound Records. *Meteorit. Planet. Sci.* **2002**, *37*(5), 661–675; doi: 10.1111/j.1945-5100.2002.tb00846.x.

[10] Martel, L.M. *Better Know A Meteorite Collection: Natural History Museum in London, United Kingdom.* Planetary Science Research Discoveries Report, 2009; p. 136.

[11] Bunch, T.E.; LeCompte, M.A.; Adedeji, A.V.; Wittke, J.H.; Burleigh, T.D.; Hermes, R.E.; Mooney, C.; Batchelor, D.; Wolbach, W.S.; Kathan, J.; et al. A Tunguska Sized Airburst Destroyed Tall el-Hammam a Middle Bronze Age city in the Jordan Valley Near the Dead Sea. *Sci. Rep*. **2021**, *11*(1):1–64; doi: 10.1038/s41598-021-97778-3.

[12] Osinski, G.R.; Eccleston, M.B.; Kleindienst, H.P.; Snith, J.R.; Boslough, M.B.E.; Schwarcz, H.; Kleindienst, M.R.; Haldemann, A.F.C.; Churcher, C.S. The Dakhleh Glass: Product of an Impact Airburst or Cratering Event in the Western Desert of Egypt? *Meteorit. Planet. Sci.* **2008**, *43*(12), 2089–2106; doi: 10.1111/j.1945-5100.2008.tb00663.x.

[13] Harris, R.; Schultz, P. Evidence of Multiple Cometary Airbursts During the Pleistocene from Pica (Chile), Dakhleh (Egypt), and Edeowie (Australia) Glasses. In *Lunar and Planetary Science Conference*; 2020; No. 2326, p. 2229.

[14] Smith, J.R.; Kleindienst, M.R.; Schwarcz, H.; Churcher, C.S.; Kieniewicz, J.M.; Osinski, G.R.; Haldemann, A.F.C. Potential Consequences of a Mid-Pleistocene Impact Event for the Middle Stone Age Occupants of Dakhleh Oasis, Western Desert, Egypt. *Quat. Int*. **2009**, *195*(1-2), 138–149; doi: 10.1016/j.quaint.2008.02.005.

[15] Osinski, G.; Haldemann, A.F.C.; Schwacz, H.P; Smith, J.R.; Kleindienst, J.M.; Kieniewicz, J.M.; Churcher, C.S. Impact Glass at the Dakhleh Oasis, Egypt: Evidence for a Cratering Event or Large Aerial Burst? In *38th Annual Lunar and Planetary Science Conference*; 2007; No. 1338; p. 1346.

[16] Harris, R.; Schultz, P. Are Ti-Rich Particles in Late Pleistocene Sediments from Patagonia Distal Ejecta from an Atacama Airburst? In *Lunar and Planetary Science Conference*; 2019; No. 2132; p. 2526.

[17] Schultz, P.; Harris, R.S.; Perroud, S.; Blanco, N.; Tomlinson, A.J.; Valenzuela, M. Late Pleistocene Fireballs Over the Atacama Desert, Chile. In *Lunar and Planetary Science Conference*; 2019; Vol. 50.

[18] Schultz, P.H.; Scott Harris, R.; Perroud, S.; Blanco, N.; Tomlinson, A.J. Widespread Glasses Generated by Cometary Fireballs During the Late Pleistocene in the Atacama Desert, Chile. *Geology.* **2022**, *50*(2), 205–209,doi: 10.1130/G49426.1.

[19] Blanco, N.; Vásquez, P.; Sepúlveda, F.A.; Tomlinson, A.J.; Quezada, A.; Ladino, M. Levantamiento geológico para el fomento de la exploración de recursos minerales e hídricos de la Cordillera de la Costa, Depresión Central y Precordillera de la Región de Tarapacá (20-21 S). Servicio Nacional de Geología y Minería, Informe Registrado IR-12-50: Santiago, 2012; Vol. 7, p. 246.

[20] Boslough, M.; Schultz, P.H.; Harris, R.S. Hypervelocity Airburst Shower Formation of the Pica Glass. In *13th Planetary Crater Consortium Meeting, 10–12 August, 2022 in Boulder, Colorado and Virtually*. LPI Contributions, 2022, Vol. 2702, p. 2021.

[21] Moore, A.M.T.; Kennett, J.P.; Napier, W.M.; Bunch, T.E.; Weaver, J.C.; LeCompte, M.; Victor Adedeji, A.; Hackley, P.; Kletetschka, G; Hermes, R.E.; et al. Evidence of Cosmic Impact at Abu Hureyra, Syria at the Younger Dryas Onset (~12.8 ka): High-Temperature Melting at >2200 °C. *Sci. Rep.* **2020**, *10*, 4185; doi: 10.1038/s41598-020-60867-w.

[22] Moore, A.M.T.; Kennett, J.P.; Napier, W.M.; Bunch, T.E.; Weaver, J.; Adedeji, A.V.; Kletetschka, G.; Hermes, R.E.; Wittke, J.H.; Razink, J.; et al. Abu Hureyra, Syria, Part 2: Additional Evidence Supporting the Catastrophic Destruction of this Prehistoric Village by a Cosmic Airburst ~12,800 Years Ago. *Airbursts Crater. Impacts*. **2023**, *1*(1), 1–36; doi: 10.14293/ACI.2023.0002.

[23] Moore, A.M.T.; Kennett, J.P.; Napier, W.M.; Bunch, T.E.; Weaver, J.C.; LeCompte, M.A.; Adedeji, A.V.; Kletetschka, G.; Hermes, R.E.; Wittke, J.H.; et al. Abu Hureyra, Syria, Part 2: Additional Evidence Supporting the Catastrophic Destruction of this Prehistoric Village by a Cosmic Airburst ~12,800 Years Ago. *Supplementary Data.* 2023. Available online: https://zenodo.org/record/8284724 (accessed on 25 August 2023).

[24] Mahaney, W.C.; Kalm, V.; Krinsley, D.; Tricart, P.; Schwartz, S.; Dohm, J.M.; Kim, K.J.; Kapran, B.; Milner, M.W.; Beukens,

R.; et al. Evidence from the Northwestern Venezuelan Andes for Extraterrestrial Impact: The Black Mat Enigma. *Geomorphology*. **2010**, *116*(1-2), 48–57; doi: 10.1016/j.geomorph.2009.10.007.

[25] Mahaney, W.C.; Krinsley, D.; Kalm, V. Evidence for a Cosmogenic Origin of Fired Glaciofluvial Beds in the Northwestern Andes: Correlation with Experimentally Heated Quartz and Feldspar. *Sediment Geol*. **2010**, *231*, 31–40; doi: 10.1016/j.sedgeo.2010.08.004.

[26] Bunch, T.E.; Hermes, R. E.; Moore, A. M.; Kennett, D. J.; Weaver, J. C.; Wittke, J. H.; DeCarli, P.S.; Bischoff, J.L.; Hillman, G.C.; Howard, G.A.; et al. Very High-Temperature Impact Melt Products as Evidence for Cosmic Airbursts and Impacts 12,900 Years Ago. *Proc. Nat. Acad. Sci. U.S.A*. **2012**, *109*(28), E1903–E1912; doi: 10.1073/pnas.1204453109.

[27] Demitroff, M.; LeCompte, M.; Rock, B. Cold Climate Related Structural Sinks Accommodate Unusual Soil Constituents, Pinelands National Reserve, New Jersey, USA. In *AGU Fall Meeting Abstracts*, 2009; pp. PP31D–1394.

[28] LeCompte, M.A.; West, A.; Adededji, A.V.; Demitroff, M.; Witwer, T.; Langenburg, R.A. The Bowser Road Mastodon and the Younger Dryas Impact Hypothesis, Appendix 3, in The Archaeological Recovery of the Bowser Road Mastodon, Orange County NY, R. Gramly, Editor. 2017, Persimmon Press: Santa Clara, CA.

[29] Koeberl, C. Libyan Desert Glass: Geochemical Composition and Origin. In *Silica'96*, 1997; p. 121–131.

[30] Svetsov, V.; Shuvalov, V.; Kosarev, I. Formation of Libyan Desert Glass: Numerical Simulations of Melting of Silica Due to Radiation from Near-Surface Airbursts. *Meteorit. Planet. Sci.* **2020**, *55*(4):895–910; doi: 10.1111/maps.13470.

[31] McHone, J.; Killgore, M.; Kudryavtsev, A. Cristobalite Inclusions in Libyan Desert Glass; Confirmation using Raman Spectroscopy. In *Lunar and Planetary Science Conference*, 2000; p. 1877.

[32] Pratesi, G.; Viti, C.; Cipriani, C.; Mellini, M. Silicate-Silicate Liquid Immiscibility and Graphite Ribbons in Libyan Desert Glass. *Geochim. Cosmochim. Acta*. **2002**, *66*(5), 903–911; doi: 10.1016/S0016-7037(01)00820-1.

[33] Kleinmann, B.; Horn, P.; Langenhorst, F. Evidence for Shock Metamorphism in Sandstones from the Libyan Desert Glass Strewn Field. *Meteorit. Planet. Sci.* **2001**, *36*(9), 1277–1282; doi: 10.1111/j.1945-5100.2001.tb01960.x.

[34] Koeberl, C.; Ferrière, L. Libyan Desert Glass Area in Western Egypt: Shocked Quartz in Bedrock Points to a Possible Deeply Eroded Impact Structure in the Region. *Meteorit. Planet. Sci.* **2019**, *54*(10), 2398–2408; doi: 10.1111/maps.13250.

[35] Aftosmis, M.J.; Mathias, D.L.; Tarano, A.M. Simulation-Based Height of Burst Map for Asteroid Airburst Damage Prediction. *Acta Astronaut*. **2019**, *156*, 278–283; doi: 10.1016/j.actaastro.2017.12.021.

[36] Artemieva, N.A.; Shuvalov, V.V. From Tunguska to Chelyabinsk via Jupiter. *Annu. Rev. Earth Planet. Sci*. **2016**, *44*, 37–56; doi: 10.1146/annurev-earth-060115-012218.

[37] Robertson, D.K.; Mathias, D.L. Hydrocode Simulations of Asteroid Airbursts and Constraints for Tunguska. *Icarus*. **2019**, *327*, 36–47; doi: 10.1016/j.icarus.2018.10.017.

[38] Boslough, M. Computational Modeling of Low-Altitude Airbursts. In *AGU Fall Meeting Abstracts*, #U21E-03, 2007.

[39] Collins, G.S.; Lynch, E.; McAdam, R.; Davison, T.M. A Numerical Assessment of Simple Airblast Models of Impact Airbursts. *Meteorit. Planet. Sci.* **2017**, *52*(8), 1542–1560; doi: 10.1111/maps.12873.

[40] Collins, G.S.; Melosh, H.J.; Marcus, R. Earth Impact Effects Program: A Web-Based Computer Program for Calculating the Regional Environmental Consequences of a Meteoroid Impact on Earth. *Meteorit. Planet. Sci.* **2005**, *40*(2), 817–840; doi: 10.1111/j.1945-5100.2005.tb00157.x.

[41] Shuvalov, V.; Artemieva, N.; Kosarev, I. 3D Hydrodynamic Code SOVA for Multimaterial Flows, Application to Shoemakerlevy 9 Comet Impact Problem. *Int. J. Impact Eng.* **1999**, *23*(1), 847–858; doi: 10.1016/S0734-743X(99)00129-3.

[42] Marcus, R.; Melosh, H.J.; Collins, G.S. Earth Impact Effects Program. 2004 2023; 2004. Available online: https://impact.ese.ic.ac.uk/ImpactEarth/ImpactEffects/ (accessed on 1 December 2023).

[43] Collins, G.S.; Melosh, H.J.; Osinski, G.R. The Impact-Cratering Process. *Elements*. **2012**, *8*(1), 25–30; doi: 10.2113/gselements.8.1.25.

[44] Mathias, D.L.; Wheeler, L.F.; Dotson, J.L. A Probabilistic Asteroid Impact Risk Model: Assessment of Sub-300 m imIacts. *Icarus*. **2017**, *289*, 106–119; doi: 10.1016/j.icarus.2017.02.009.

[45] Muthini, J.; Okeng'o, G.O. Modelling the Dynamics of Potentially Dangerous Large-Earth Impactors. arXiv preprint arXiv:2107.05988. **2021**; doi: 10.48550/arXiv.2107.05988.

[46] Osinski, G.R.; Grieve, R.A.F.; Ferrière, L.; Losiak, A.; Pickersgill, A.E.; Cavosie, A.J.; Hibbard, S.M.; Hill, P.J.A.; Bermudez, J.J.; Marion, C.L.; et al. Impact Earth: A Review of the Terrestrial Impact Record. *Earth Sci. Rev.* **2022**, *232*, 104112; doi: 10.1016/j.earscirev.2022.104112.

[47] Lv, H.; He, Q.; Chen, X.; Han, P. Numerical Simulation of Impact Crater Formation and Distribution of High-Pressure Polymorphs. *Acta Astronaut*. **2023**, *203*, 169–186; doi: 10.1016/j.actaastro.2022.11.048.

[48] Baldwin, E.; Milner, D.J.; Burchell, M.J.; Crawford, I.A. Shock wave propagation and damage to the target in oceanic impact events. In *Bridging the Gap II: Effect of Target Properties on the Impact Cratering Process*; 2007; No. 1360; pp. 13–14.

[49] Baldwin, E.; Vocadlo, L.; Crawford, I. Validation of AUTODYN in Replicating Large-Scale Planetary Impact Events. In *36th Annual Lunar and Planetary Science Conference*, 2005, p. 1380.

[50] Saito, T.; Kaiho, K.; Abe, A.; Katayama, M. Hypervelocity Impact of Asteroid/Comet on the Ceanic Crust of the Earth. *Int. J. Impact Eng.* **2008**, *35*(12), 1770–1777; doi: 10.1016/j.ijimpeng.2008.07.046.

[51] Saito, T.; Kaiho, K.; Abe, A.; Katayama, M.; Takayama, K. Numerical Simulations of Hypervelocity Impact of Asteroid/Comet on the Earth. *Int. J. Impact Eng.* **2006**, *33*(1–12), 713–722; doi: 10.1016/j.ijimpeng.2006.09.012.

[52] Birnbaum, N.K.; Cowler, M.; Hayhurst, C. Numerical Simulation of Impact using AUTODYN. In *Proc. 2nd Int. Impact Sympo.*; Beijing, China, 1996.

[53] Deller, J.F.; Lowry, S.C.; Snodgrass, C.; Price, M.C.; Sierks, H. A New Approach to Modelling Impacts on Rubble Pile Asteroid Simulants. *Mon. Not. R. Astron. Soc.* **2016**, *455*(4), 3752–3762; doi: 10.1093/mnras/stv2584h.

[54] Jones, A.P.; Price, D.G.; DeCarli, P.S.; Price, N.; Clegg, R. Impact Decompression Melting: A Possible Trigger for Impact Induced Volcanism and Mantle Hotspots? In *Impact Markers in the Stratigraphic Record;* 2003; pp. 91–119; doi: 10.1007/978-3-642-55463-6_4.

[55] Nishizawa, M.; Matsui, Y.; Suda, K.; Saito, T.; Shibuya, T.; Takai, K.; Hasegawa, S.; Yano, H. Experimental Simulations of Hypervelocity Impact Penetration of Asteroids into the Terrestrial Ocean and Benthic Cratering. *J. Geophys. Res. Planets* **2020**, *125*(12), e2019JE006291; doi: 10.1029/2019JE006291.

[56] Stickle, A.M.; Barnouin, O.S.; Syal, M.B.; Cheng, A.; El-Mir, C.; Ernst, C.M.; Michel, P.; Oklay, N.; Owen, M.; Price, M.; et al. Impact Simulation Benchmarking for the Double Asteroid Redirect Test (DART). In *47th Annual Lunar and Planetary Science Conference*; 2016; No. 1903, p. 2832.

[57] Wie, B. *An Innovative Solution to NASA's NEO Impact Threat Mitigation Grand Challenge and Flight Validation Mission Architecture Development*. 2014.

[58] Caldwell, W.K.; Euser, B.; Plesko, C.S.; Larmat, C.; Lei, Z.; Knight, E.E.; Rougier, E.; Hunter, A. Benchmarking Numerical Methods for Impact and Cratering Applications. *Appl. Sci.* **2021**, *11*(6), 2504; doi: 10.3390/app11062504.

[59] Birnbaum, N.; Cowler, M.S.; Itoh, M.; Katayama, M.; Obata, H. AUTODYN-An Interactive Non-Linear Dynamic Analysis Program for Microcomputers through Supercomputers. In *Transactions of the 9th International Conference on Structural Mechanics in Reactor Technology*; 1987; Volume B.

[60] Pierazzo, E.; Artemieva, N.; Asphaug, E.; Baldwin, E.C.; Cazamias, J.; Coker, R.; Collins, G.S.; Crawford, D.A.; Davison, T.; Elbeshausen, D.; et al. Validation of Numerical Codes for Impact and Explosion Cratering: Impacts on Strengthless and Metal Targets. *Meteorit. Planet. Sci.* **2008**, *43*(12), 1917–1938; doi: 10.1111/j.1945-5100.2008.tb00653.x.

[61] Svetsov, V.V.; Shuvalov, V.V.; Artemieva, N.A.; Khazins, V.M.; Popova, O.P.; Glazachev, D.O.; Podobnaya, E.D. Complex Assessment of Hazardous Effects of Impacts of Cosmic Objects. In *81st Annual Meeting of the Meteoritical Society*, 2018; Volume 81, No. 2067, p. 6145.

[62] Shuvalov, V.V.; Trubetskaya, I.A. Aerial Bursts in the Terrestrial Atmosphere. *Sol. Syst. Res.* **2007**, *41*, 220–230; doi: 10.1134/S0038094607030057.

[63] Florenskiy, K. Preliminary Results from the 1961 Combined Tunguska Meteorite Expedition. *Meteoritica* **1965**, *XXIII*(23), 3–37.

[64] Svetsov, V.B. Thermal Radiation on the Ground from Large Aerial Bursts Caused by Tunguska-Like Impacts. *Lunar and Planetary Science XXXVII* **2006**, *2006*, 1–2.

[65] Wolbach, W.S.; Ballard, J.P.; Mayewski, P.A.; Parnell, A.C.; Cahill, N.; Adedeji, V.; Bunch, T.E.; Domínguez-Vázquez, G.; Erlandson, J.M.; Firestone, R.B.; et al. Extraordinary Biomass-Burning Episode and Impact Winter Triggered by the Younger Dryas Cosmic Impact ~12,800 Years Ago. 2. Lake, Marine, and Terrestrial Sediments. *J. Geol.* **2018**, *126*(2), 185–205; doi: 10.1086/695704.

[66] Longo, G. The Tunguska Event. In *Comet/Asteroid Impacts and Human Society*; An Interdisciplinary Approach, 2007; pp. 303–330; doi: 10.1007/978-3-540-32711-0_18.

[67] Jenniskens, P.; Popova, O.P.; Glazachev, D.O.; Podobnaya, E.D.; Kartashova, A.P. Tunguska Eyewitness Accounts, Injuries, and Casualties. *Icarus* **2019**, *327*, 4–18; doi: 10.1016/j.icarus.2019.01.001.

[68] Kletetschka, G.; Vyhnanek, J.; Kawasumiova, D.; Nabelek, L.; Petrucha, V. Localization of the Chelyabinsk Meteorite from Magnetic Field Survey and GPS Data. *IEEE Sens. J.* **2015**, *15*(9), 4875–4881; doi: 10.1109/JSEN.2015.2435252.

[69] Brown, P.G.; Assink, J.D.; Astiz, L.; Blaauw, R.; Boslough, M.B.; Borovička, J.; Brachet, N.; Brown, D.; Campbell-Brown, M.; Ceranna, L.; et al. A 500-Kiloton Airburst Over Chelyabinsk and an Enhanced Hazard from Small Impactors. *Nature* **2013**, *503*(7475), 238–241; doi: 10.1038/nature12741.

[70] Popova, O.P.; Jenniskens, P.; Emel'yanenko, V.; Kartashova, A.; Biryukov, E.; Khaibrakhmanov, S.; Shuvalov, V.; Rybnov, Y.; Dudorov, A.; Grokhovsky, V.I.; et al. Chelyabinsk Airburst, Damage Assessment, Meteorite Recovery, and Characterization. *Science* **2013**, *342*(6162), 1069–1073; doi: 10.1126/science.1242642.

[71] Kocherov, A.; Korochantsev, A.V.; Lorenz, C.A.; Ivanova, M.A.; Grokhovsky, V.I. Recovery, Laboratory Preparation and Current State of the Main Mass of the Chelyabinsk Meteorite. In *45th Annual Lunar and Planetary Science Conference*; 2014; No. 1777, p. 2227.

[72] Marley, W.; Penney, W.; Reines, F. July 16th Nuclear Explosion: Measurement of Maximum Blast Pressure Near the Center, Los Alamos Scientific Laboratory Report LA-431. In *Los Alamos Scientific Laboratory report LA-431*; Los Alamos, NM, 1946; p. 10.

[73] Hermes, R.E.; Wenk, H.-R.; Kennett, J.P.; Bunch, T.E.; Moore, C.R.; LeCompte, M.A.; Kletetschka, G.; Adedeji, A.V.; Langworthy, K.; Razink, J.J.; et al. Microstructures in Shocked Quartz: Linking Nuclear Airbursts and Meteorite Impacts. *ScienceOpen* **2023**, *1*(1); doi: 10.14293/ACI.2023.0001.

[74] Donohue, P.H.; Simonetti, A. Vesicle Size Distribution as a Novel Nuclear Forensics Tool. *PLoS One* **2016**, *11*(9), e0163516; doi: 10.1371/journal.pone.0163516.

[75] Eby, G.N.; Charnley, N.; Pirrie, D.; Hermes, R.; Smoliga, J.; Rollinson, G. Trinitite Redux: Mineralogy and Petrology. *Am. Min.* **2015**, *100*(2–3), 427–441; doi: 10.2138/am-2015-4921.

[76] Lussier, A.J.; Rouvimov, S.; Burns, P.C.; Simonetti, A. Nuclear-Blast Induced Nanotextures in Quartz and Zircon within Trinitite. *Am. Min.* **2017**, *102*(2), 445–460; doi: 10.2138/am-2017-5739.

[77] Sharp, N.; McDonough, W.F.; Ticknor, B.W.; Ash, R.D.; Piccoli, P.M.; Borg, D.T. Rapid Analysis of Trinitite with Nuclear Forensic Applications for Post-Detonation Material Analyses. *J. Radioanal. Nucl. Chem.* **2014**, *302*(1), 57–67; doi: 10.1007/s10967-014-3285-9.

[78] Day, J.M.; Moynier, F.; Meshik, A.P.; Pradivtseva, O.V.; Petit D.R. Evaporative Fractionation of Zinc during the First Nuclear Detonation. *Sci. Adv.* **2017**, *3*(2), e1602668; doi: 10.1126/sciadv.1602668.

[79] Bindi, L.; Kolb, W.; Eby, G.N.; Asimow, P.D.; Wallace, T.C.; Steinhardt, P.J. Accidental Synthesis of a Previously Unknown Quasicrystal in the First Atomic Bomb Test. *Proc. Natl. Acad. Sci. U.S.A.* **2021**, *118*(22), e2101350118; doi: 10.1073/pnas.2101350118.

[80] Taylor, G.I. The Formation of a Blast Wave by a very Intense Explosion I. Theoretical Discussion. In *Proceedings of the Royal Society of London. Series A. Mathematical and Physical Sciences*; 1950; Volume 201(1065), pp. 159–174; doi: 10.1098/rspa.1950.0049.

[81] Glasstone, S.; Dolan, P.J. *The Effects of Nuclear Weapons*, 3rd ed.; US Dept of Defense, U.S. Government Printing Office: Washington, DC, 1977; doi: 10.2172/6852629.

[82] Brode, H.L. *Airblast from Nuclear Bursts–Analytic Approximations*; Pacific-Sierra Research Corporation.

[83] Kraus, R.G.; Stewart, S.T.; Swift, D.C.; Bolme, C.A.; Smith, R.F.; Hamel, S.; Hammel, B.D.; Spaulding, D.K.; Hicks, D.G.; Eggert, J.H.; et al. Shock Vaporization of Silica and the Thermodynamics of Planetary Impact Events. *J. Geophys. Res. Planets* **2012**, *117*(E9); doi: 10.1029/2012JE004082.

[84] Ben Younes, M.E.; Grégoire, D.C.; Chakrabarti, C.L. Vaporization and Removal of Silica for the Direct Analysis of Geological Materials by Slurry Sampling Electrothermal Vaporization-Inductively Coupled Plasma-Mass Spectrometry. *J. Anal. At. Spectrom.* **1999**, *14*(11), 1703–1708; doi: 10.1039/A903269J

[85] Kieffer, S.W. Shock Metamorphism of the Coconino Sandstone at Meteor Crater, Arizona. *J. Geophys. Res.* **1971**, *76*(23), 5449–5473; doi: 10.1029/JB076i023p05449.

[86] Kieffer, S.W.; Phakey, P.P.; Christie, J.M. Shock Processes in Porous Quartzite: Transmission Electron Microscope Observations and Theory. *Contrib. Mineral. Petrol.* **1976**, *59*(1), 41–93; doi: 10.1007/BF00375110.

[87] Wakita, S.; Johnson, B.C.; Denton, C.A.; Davison, T.M. Jetting During Oblique Impacts of Spherical Impactors. *Icarus* **2021**, *360*, 114365; doi: 10.1016/j.icarus.2021.114365.

[88] Ernstson, K. *Meteorite Impact Spallation: From Mega- to Micro-Scale*. Ernstson Claudin Impact Structures - Meteorite Craters 2014. Available online: http://www.impact-structures.com/impact-educational/meteorite-impact-spallation-from-mega-to-micro-scale/ (3 May 2023).

[89] Ernstson, K. Evidence of Meteorite Impact-Induced Thermal Shock in Quartz. In *Modern Problems of Theoretical, Experimental, and Applied Mineralogy*; 2020; p. 1423.

[90] Koeberl, C. The Geochemistry and Cosmochemistry of Impacts. In *Planets, Asteriods, Comets and the Solar System*; 2014; pp. 73–118.

[91] Christie, J.; Ardell, A. Substructures of Deformation Lamellae in Quartz. *Geology*, **1974**, *2*(8), 405–408; doi: 10.1130/0091-7613(1974)2[[405:SODLIQ]]2.0.CO;2.

[92] Kowitz, A.; Güldemeister, N.; Schmitt, R.T.; Reimold, W.-U.; Wünnemann, K.; Holzwarth, A. Revision and Recalibration of Existing Shock Classifications for Quartzose Rocks using Low-Shock Pressure (2.5–20 GPa) Recovery Experiments and Mesoscale Numerical Modeling. *Meteorit. Planet. Sci.* **2016**, *51*(10), 1741–1761; doi: 10.1111/maps.12712.

[93] Kowitz, A.; Schmitt, R.T.; Uwe Reimold, W.; Hornemann, U. The First MEMIN Shock Recovery Experiments at Low Shock Pressure (5–12.5 GPa) with Dry, Porous Sandstone. *Meteorit. Planet. Sci.* **2013**, *48*(1), 99–114; doi: 10.1111/maps.12030.

[94] Kowitz, A.; Güldemeister, N.; Reimold, W.U.; Schmitt, R.T.; Wünnemann, K. Diaplectic Quartz Glass and SiO_2 Melt Experimentally Generated at only 5 GPa Shock Pressure in Porous Sandstone: Laboratory Observations and Meso-Scale Numerical Modeling. *Earth Planet. Sci. Lett.* **2013**, *384*, 17–26; doi: 10.1016/j.epsl.2013.09.021.

[95] Stöffler, D.; Gault, D.E.; Wedekind, J.; Polkowski, G. Experimental Hypervelocity Impact into Quartz Sand: Distribution and Shock Metamorphism of Ejecta. *J. Geophys. Res.* **1975**, *80*(29), 4062–4077; doi: 10.1029/JB080i029p04062.

[96] Ebert, M.; Hecht, L.; Deutsch, A.; Kenkmann, T. MEMIN: Chemical Modification of Projectile Spheres, Target Melts and Shocked Quartz in Hypervelocity Impact Experiments. In *42nd Annual Lunar and Planetary Science Conference*; 2011; No. 1608, p. 1400.

[97] Boslough, M.B.; Cygan, R.T.; Crawford, D.A.; Kirkpatrick, R.J. NMR Spectroscopy of Shocked Quartz from Experimental Impact Craters. *Lunar Planet. Sci.* **1996**, *27*, 137–138.

[98] Wünnemann, K.; Zhu, M.H.; Stöffler, D. Impacts into Quartz Sand: Crater Formation, Shock Metamorphism, and Ejecta Distribution in Laboratory Experiments and Numerical Models. *Meteorit. Planet. Sci.* **2016**, *51*(10), 1762–1794; doi: 10.1111/maps.12710.

[99] Silber, E.A.; Boslough, M.; Hocking, W.K.; Gritsevich, M.; Whitaker, R.W. Physics of Meteor Generated Shock Waves in the Earth's Atmosphere–A Review. *Adv. Space Res.* **2018**, *62*(3), 489–532; doi: 10.1016/j.asr.2018.05.010.

[100] Zhilyaev, B.; Petukhov, V.N.; Reshetnyk, V.N.; Vidmachenko, A.P. Meteor Colorimetry with CMOS Cameras. arXiv preprint arXiv:2106.07403, 2021.

[101] West, A.; Young, M.D.; Costa, L.; Kennett, J.P.; Moore, C.R.; LeCompte, M.A.; Kletetschka, G.; Hermes, R.E. Modeling Airbursts by Comets, Asteroids, and Nuclear Detonations: Shock Metamorphism, Meltglass, and Microspherules. *Airburst. Crater. Imp.* **2024**, *2*, 1–30.

[102] Molnár, M.; Ventura, K.; Svanda, P.; Štaffen, Z.; Rappenglück, M.A.; Ernstson, K. Chrudim-Pardubice: Evidence for a Young Meteorite Impact Strewn Field in the Czech Republic. In *48th Annual Lunar and Planetary Science Conference*; 2017; No. 1964, p. 1920.

[103] Poßekel, J.; Molnár, M.; Ernstson, K. The Proposed Meteorite Impact Event in the Czech Republic: Evidence Strengthened by Investigations with the Digital Terrain Model. In *53rd Lunar and Planetary Science Conference*; 2022; Abstract 2678, p. 1558.

[104] Ernstson, K.; Müller, W.; Gawlik-Wagner, A. The Saarlouis semi crater structure: notable insight into the Saarland (Germany) meteorite impact event achieved, Abstract and Poster #1876. In *49th Lunar and Planetary Science Conference*; 2018; Abstract 1876.

[105] Ernstson, K.; Portz, D.; Müller, W. Zhamanshinite-Like Black-Glass Melt Rocks from the Saarland (Germany) Meteorite Impact Site. In *52nd Lunar and Planetary Science Conference*; 2021; No. 2548, p. 1350.

[106] Siegel, U.; Müller, W.; Michelbacher, S.; Ernstson, K.; Rommelfangen, J. Shatter Cones in Litermont Quartzites: Saarlouis/Nalbach (Saarland, Germany) Meteorite Impact Event Strengthened. In *Lunar and Planetary Science Conference*; 2022; Abstract 1842; doi: 10.13140/RG.2.2.34259.86568.

[107] Ernstson, K.; Bauer, F.; Hiltl, M. A Prominent Iron Silicides Strewn Field and Its Relation to the Bronze Age/Iron Age Chiemgau Meteorite Impact Event (Germany). *Earth Sci.* **2023**, *12*(1), 26–40; doi: 10.11648/j.earth.20231201.14.

[108] Ernstson, K.; Mayer, W.; Neumair, A.; Rappenglueck, B.; Rappenglück, M.A.; Sudhaus, D.; Zeller, K.W. The Chiemgau Crater Strewn Field: Evidence of a Holocene Large Impact Event in Southeast Bavaria, Germany. *J. Sib. Fed.* **2010**, *1*(3), 72–103.

[109] Ernstson, K.; Poßekel, J.; Rappenglück, M.A. Near-Ground Airburst Cratering: Petrographic and Ground Penetrating Radar (GPR) Evidence for a Possibly Enlarged Chiemgau Impact Event (Bavaria, SE-Germany). In *Lunar and Planetary Science Conference*; 2020; No. 2326, p. 1231.

[110] Ernstson, K.; Sideris, C.; Liritzis, I.; Neumair, A. The Chiemgau Meteorite Impact Signature of the Stöttham Archaeological Site (Southeast Germany). *Mediterr. Archaeol. Archaeom.* **2012**, *12*(2), 249–259.

[111] Rappenglück, B.; Hiltl, M.; Ernstson, K. Artifact-In-Impactite: A New Kind of Impact Rock. Evidence from the Chiemgau Meteorite Impact in Southeast Germany. In *Proceedings of the Modern Problems of Theoretical, Experimental, and Applied Mineralogy*, Yushkin Readings – 7–10 December 2020, Syktyvkar, Russia; 2020; pp. 365–367.

[112] Rappenglück, B.; Hiltl, M.; Ernstson, K. Metallic Artifact Remnants in a Shock-Metamorphosed Impact Breccia: an Extended View of the Archeological Excavation at Stöttham (Chiemgau, SE-Germany). In *50th Annual Lunar and Planetary Science Conference*; 2019; No. 2132, p. 1334.

[113] Rappenglück, M.A.; Ernstson, K.; Mayer, W.; Beer, R.; Benske, G.; Siegl, C.; Sporn, R.; Bliemetsrieder, T.; Schüssler, U. *The Chiemgau Impact Event in the Celtic Period: Evidence of a Crater Strewn Field and a Cometary Impactor Containing Presolar Matter*. Chiemgau-Impakt c/o Kord Ernstson, 2004.

[114] Rappenglück, B.; Hiltl, M.; Poßekel, J.; Rappenglück, M.A.; Ernstson, K. People Experienced the Prehistoric Chiemgau Meteorite Impact – Geoarchaeological Evidence from Southeastern Germany: a Review. *Mediterr. Archaeol. Archaeom.* **2023**, *23*(1), 209–234; doi: 10.5281/zenodo.7775799.

[115] Rappenglück, B.; Hiltl, M.; Ernstson, K. Exceptional Evidence of a Meteorite Impact at the Archaeological Site of Stöttham (Chiemgau, SE-Germany). In *Harmony and Symmetry: Celestial Regularities Shaping Human Culture. Proceedings of the SEAC 2018 Conference*; Draxler, S.; Lippitsch, M.E.; Wolfschmidt, G.; Eds.; Tredition: Hamburg, 2020; pp. 116–125.

[116] Rappenglück, B.; Hiltl, M.; Ernstson, K. The Chiemgau Impact: Evidence of a Latest Bronze Age/Early Iron Age Meteorite Impact in the Archaeological Record, and Resulting Critical Considerations of Catastrophism. In *Beyond Paradigms in Cultural Astronomy*; González-García, C.; Frank, R.M.; Sims, L.D.; Rappenglück, M.A.; Zotti, G.; Belmonte, J.A.; Šprajc, I.; Eds.; 2021; pp. 57–64.

[117] Ernstson, K.; Shumilova, T.G. Chiemite—A High PT Carbon Impactite from Shock Coalification/carbonization of Impact Target Vegetation. In *Conference: Modern Problems of Theoretical, Experimental, and Applied Mineralogy (Yushkin Readings — 2020)*; Syktyvkar, Russia, 2020.

[118] Waldmann, G.; Herten, F.; Hiltl, M.; Ernstson, K. The Enigmatic Niederrhein (Germany) Deposit: Evidence of a Middle-Pleistocene Meteorite Impact Strewn Field. In *49th Annual Lunar and Planetary Science Conference*; 2018; No. 2083, p. 1610.

[119] Andronikov, A.V.; Andronikova, I.E. Sediments from Around the Lower Younger Dryas Boundary (USA): Implications from LA-ICP-Analysis. *Geogr. Ann. A* **2016**, *98*, pp. 221–236; doi: 10.1111/geoa.12132.

[120] Ballard, J.P.; Bijkerk, A.K. Quartz Melt Structures in European Coversands May Support Younger Dryas Extraterrestrial Impact Hypothesis. In *UT Geography Research Symposium 2014 "Mapping Outside the Lines: Geography as a Nexus for Interdisciplinary and Collaborative Research*"; Knoxville, Tennessee, 2014.

[121] Bement, L.C.; Madden, A.S.; Carter, B.J.; Simms, A.R.; Swindle, A.L.; Alexander, H.M.; Fine, S.; Benamara, M. Quantifying the Distribution of Nanodiamonds in Pre-Younger Dryas to Recent Age Deposits Along Bull Creek, Oklahoma Panhandle, USA. *Proc. Nat. Acad. Sci.* **2014**, *111*(5), pp. 1726–1731; doi: 10.1073/pnas.1309734111.

[122] Firestone, R.B.; West, A.; Kennett, J.P.; Becker, L.; Bunch, T.E.; Revay, Z.S.; Schultz, P.H.; Belgya, T.; Kennett, D.J.; Erlandson, J.M.; et al. Evidence for an Extraterrestrial Impact 12,900 Years ago that

Contributed to the Megafaunal Extinctions and the Younger Dryas Cooling. *Proc. Nat. Acad. Sci*. **2007**, *104*(41), pp. 16016–16021; doi: 10.1073/pnas.0706977104.

[123] Israde-Alcántara, I.; Bischoff, J.L.; Domínguez-Vázquez, G.; Li, H.C.; DeCarli, P.S.; Bunch, T.E.; Wittke, J.H.; Weaver, J.C.; Firestone, R.B.; West, A.; et al. Evidence from Central Mexico Supporting the Younger Dryas Extraterrestrial Impact Hypothesis. *Proc. Nat. Acad. Sci.* **2012**, *109*(13), pp. E738–E747; doi: 10.1073/pnas.1110614109.

[124] LeCompte, M.A.; Goodyear, A.C.; Demitroff, M.N.; Batchelor, D.; Vogel, E.K.; Mooney, C.; Rock, B.N.; Seidel, A.W. Independent Evaluation of Conflicting Microspherule Results from Different Investigations of the Younger Dryas Impact Hypothesis. *Proc. Nat. Acad. Sci*. **2012**, *109*(44), pp. E2960–E2969; doi: 10.1073/pnas.1208603109.

[125] Moore, A.M.T.; Kennett, J.P.; LeCompte, M.A.; Moore, C.R.; Li, Y.Q.; Kletetschka, G.; Langworthy, K.; Razink, J.J.; Brogden, V.; van Devener, B.; et al. Abu Hureyra, Syria, Part 1: Shock-Fractured Quartz Grains Support 12,800-Year-Old Cosmic Airburst at the Younger Dryas Onset. *ScienceOpen* **2023**, *1*(1), 1–28.

[126] Moore, C.R.; West, A.; LeCompte, M.A.; Brooks, M.J.; Daniel, I.R. Jr.; Goodyear, A.C.; Ferguson, T.A.; Ivester, A.H.; Feathers, J.K.; Kennett, J.P.; et al. Widespread Platinum Anomaly Documented at the Younger Dryas Onset in North American Sedimentary Sequences. *Sci. Rep.* **2017**, *7*, 44031; doi: 10.1038/srep44031.

[127] Teller, J.; Boyd, M.; LeCompte, M.; Kennett, J.; West, A.; Telka, A.; Diaz, A.; Adedeji, V.; Batchelor, D.; Mooney, C. A Multi-Proxy Study of Changing Environmental Conditions in a Younger Dryas Sequence in Southwestern Manitoba, Canada, and Evidence for an Extraterrestrial Event. *Quat. Res*. **2019**, *93*, 1–28; doi: 10.1017/qua.2019.46.

[128] Wolbach, W.S.; Ballard, J.P.; Mayewski, P.A.; Adedeji, V.; Bunch, T.E.; Firestone, R.B.; French, T.A.; Howard, G.A.; Israde-Alcántara, I.; Johnson, J.R.; et al. Extraordinary Biomass-Burning Episode and Impact Winter Triggered by the Younger Dryas Cosmic Impact ~12,800 Years Ago. 1. Ice Cores and Glaciers. *J. Geol.* **2018**, *126*(2), 165–184; doi: 10.1086/695703.

[129] Moore, A.M.T.; Kennett, J.P.; Napier, W.M.; LeCompte, M.A.; Moore, C.R.; West, A. Abu Hureyra, Syria, Part 3: Comet Airbursts Triggered Major Climate Change 12,800 Years ago That Initiated the Transition to Agriculture. *ScienceOpen* **2023**, *1*(1), 1–24; doi: 10.14293/ACI.2023.0004.

[130] Moore, C.R.; Brooks, M.J.; Goodyear, A.C.; Ferguson, T.A.; Perrotti, A.G.; Mitra, S.; Listecki, A.M.; King, B.C.; Mallinson, D.J.; Lane, C.S.; et al. Sediment Cores from White Pond, South Carolina, Contain a Platinum Anomaly, Pyrogenic Carbon Peak, and Coprophilous Spore Decline at 12.8 ka. *Sci. Rep.* **2019**, *9*(1), 15121; doi: 10.1038/s41598-019-51552-8.

[131] Moore, C.R.; Brooks, M.J.; Dunbar, J.S.; Hemmings, C.A.; Feathers, J.K. Geoarchaeological Investigations at Wakulla Springs, Florida. Southeastern Archaeological Conference (SEAC). In Proceedings of the 76th Annual Meeting, November 6–9, 2019.

[132] Pino, M.; Abarzúa, A.M.; Astorga, G.; Martel-Cea, A.; Cossio-Montecinos, N.; Navarro, R.X.; Lira, M.P.; Labarca, R.; LeCompte, M.A.; Adedeji, V.; et al. Sedimentary Record from Patagonia, Southern Chile Supports Cosmic-Impact Triggering of Biomass Burning, Climate Change, and Megafaunal Extinctions at 12.8 ka. *Sci. Rep.* **2019**, *9*(1), 4413; doi: 10.1038/s41598-018-38089-y.

[133] Wittke, J.H.; Weaver, J.C.; Bunch, T.E.; Firestone, R.B. Evidence for Deposition of 10 Million Tonnes of Impact Spherules Across Four Continents 12,800 y ago. *Proc. Nat. Acad. Sci.* **2013**, *110*(23), E2088–E2097; doi: 10.1073/pnas.13017601.

[134] Napier, W.M. Palaeolithic Extinctions and the Taurid Complex. *Mon. Not. R Astron. Soc.* **2010**, *405*, 1901–1906; doi: 10.1111/j.1365-2966.2010.16579.x.

[135] Napier, W.M. The Hazard from Fragmenting Comets. *Mon. Not. R Astron. Soc*. **2019**, *488*(2), 1822–1827; doi: 10.1093/mnras/stz1769.

[136] van Ginneken, M.; Folco, L.; Perchiazzi, N.; Rochette, P.; Bland. P.A. Meteoritic ablation debris from the Transantarctic Mountains: Evidence for a Tunguska-like impact over Antarctica ca. 480 ka ago. *Earth Planet. Sci. Lett*. **2010**, *293*(1–2), 104–113; doi: 10.1016/j.epsl.2010.02.028.

[137] van Ginneken, M.; Suavet, C.; Cordier, C.; Folco, L.; Rochette, P.; Sonzogni, C.; Perchiazzi, N. Oxygen Isotope Composition of Meteoritic Ablation Debris from the Transantarctic Mountains: Constraining the Parent Body and Implications for the Impact Scenario. *Meteorit. Planet. Sci*. **2012**, *47*(11), 1738–1747; doi: 10.1111/maps.12011.

[138] Ernstson, K.; Schulz-Hertlein, G.; Poßekel, J.; Ernstson, T. A Probable Holocene Meteorite Impact Crater Strewn Field in Lower Franconia (Germany): Evidence from Digital Terrain Models and Geophysical Surveys (GPR, Electrical Imaging, Geomagnetics). In *Poster, Proceedings of the AGU Fall Meeting*; 2022.

[139] Ernstson, K.; Poßekel, J.; Kurtz, J. The Enigmatic Sachsendorf Bay Structure (Oderbruch, Northeast Germany): Evidence of a Pleistocene/Holocene Meteorite Impact Event. In *12th Planetary Crater Consortium Meeting*; 2021; Vol. 12, No. 2621, p. 2022.

[140] Molnár, M.; Ventura, K.; Poßekel, J.; Ernstson, K. *The Kolešovice 20 km-Diameter Structure (Czech Republic): Evidence of an Airburst Impact Crater.* LPI Contributions; 2023; No. 2806, p. 1428.

[141] Ahokas, H. *Thirty-three Previously Unknown Meteoritic Craters of Diameter from 5 to 100 m in Western Kouvola, Finland from a Swarm of Impactors in the Holocene*, Kave: Helsinki, 2023; p. 38.

[142] Shumilova, T.G.; Isaenko, S.I.; Ulyashev, V.V.; Makeev, B.A.; Rappenglück, M.A.; Veligzhanin, A.A.; Ernstson, K. Enigmatic Glass-Like Carbon from the Alpine Foreland, Southeast Germany: A Natural Carbonization Process. *Acta Geol. Sin.* **2018**, *92*(6), 2179–2200; doi: 10.1111/1755-6724.13722.

[143] Bailey, B.K.; Cohen, A.N.; Patel, D.; Lubin, P.; Boslough, M.; Robertson, D.; Egan, S.; Khetia, J.; Costa, T.; Silber, E.; et al. Asteroid 2023 NT1: A Cautionary Tale. arXiv preprint arXiv:2310.13112, 2023; doi: 10.48550/arXiv.2310.13112.

[144] Bailey, B.K.; Cohen, A.N.; Patel, D.; Lubin, P.; Boslough, M.; Robertson, D.; Egan, S.; Khetia, J.; Costa, T.; Silber, E.A.; et al. Asteroid 2023 NT1–A Cautionary Tale. AGU23, iPoster: San Francisco, CA, 2023.

[145] Marcus, R.; Melosh, H.J.; Collins. G.S. Earth Impact Effects Program, Examples. 2004 [cited 2024 April, 2024]; Available online: https://impact.ese.ic.ac.uk/ImpactEarth/ImpactEffects/examples.html (accessed on 22 January 2024).

[146] Ferus, M.; Knížek, A.; Cassone, G.; Rimmer, P.B.; Changela, H.; Chatzitheodoridis, E.; Uwarova, I.; Žabka, J.; Kabáth, P.; Saija, F. et al. Simulating Asteroid Impacts and Meteor Events by High-Power Lasers: From the Laboratory to Spaceborne Missions. *Front. Astron. Space Sci.* **2023**, *10*, 1–12; doi: 10.3389/fspas.2023.1186172.

[147] Artemieva, N.; Pierazzo, E.; The Canyon Diablo Impact Event: 2. Projectile Fate and Target Melting Upon Impact. *Meteorit. Planet. Sci*. **2011**, *46*(6), 805–829; doi: 10.1111/j.1945-5100.2011.01195.x.

[148] Koeberl, C.; Claeys, P.; Hecht, L.; Mcdonald, I. Geochemistry of Impactites. *Elements* **2012**, *8*(1), 37–42; doi: 10.2113/gselements.8.1.37.